https://doi.org/10.5194/acp-2021-700
Preprint. Discussion started: 6 September 2021


Atmospheric Chemistry and Physics Discussions

# Circum-Antarctic abundance and properties of CCN and INP

Christian Tatzelt[1], Silvia Henning[1], André Welti[2], Andrea Baccarini[3,4], Markus Hartmann[1], Martin Gysel-Beer[3], Manuela van Pinxteren[1], Robin L. Modini[3], Julia Schmale[3,4], and Frank Stratmann[1]

[1]Leibniz Institute for Tropospheric Research, Permoserstrasse 15, 04318 Leipzig, Germany
[2]Finnish Meteorological Institute, Erik Palménin aukio 1, FI-00560 Helsinki, Finland
[3]Laboratory of Atmospheric Chemistry, Paul Scherrer Institute, 5232 Villigen PSI, Switzerland
[4]Extreme Environments Research Laboratory, École Polytechnique Fédérale de Lausanne, School of Architecture, Civil and Environmental Engineering, Lausanne, Switzerland

**Correspondence:** Silvia Henning (silvia.henning@tropos.de), Julia Schmale (julia.schmale@epfl.ch)

**Abstract.** Aerosol particles acting as cloud condensation nuclei (CCN) or ice nucleating particles (INP) play a major role in the formation and glaciation of clouds. Thereby they exert a strong impact on the radiation budget of the Earth. Data on abundance and properties of both types of particles are sparse, especially for remote areas of the world, such as the Southern Ocean (SO). In this work, we present unique results from ship-borne aerosol-particle-related in situ measurements and filter sampling in the SO region, carried out during the Antarctic Circumnavigation Expedition (ACE) in the Austral summer of 2016/17. An overview of CCN and INP concentrations on the Southern Ocean is provided and using additional quantities, insights regarding possible CCN and INP sources and origins are presented. CCN number concentrations spanned 2 orders of magnitude, e.g., for a supersaturation of $0.3\,\%$ values ranged roughly from 3 to $590\,\mathrm{cm}^{-3}$. CCN showed variable contributions of organic and inorganic material (inter-quartile range of hygroscopicity parameter $\kappa$ from 0.2 to 0.9). No distinct size-dependence of $\kappa$ was apparent, indicating homogeneous composition across sizes (critical dry diameter on average between 37 and $123\,\mathrm{nm}$). The contribution of sea spray aerosol (SSA) to the CCN number concentration was on average small. Ambient INP number concentrations were measured in the temperature range from $-5$ to $-27^{\circ}\mathrm{C}$. Concentrations spanned up to 3 orders of magnitude, e.g., at $-16^{\circ}\mathrm{C}$ from 0.2 to $100\,\mathrm{m}^{-3}$. Elevated values (above $10\,\mathrm{m}^{-3}$ at $-16^{\circ}\mathrm{C}$) were measured when the research vessel was in the vicinity of land, with lower and more constant concentrations when at sea. This hints towards terrestrial and/or coastal INP sources being dominant close to land. In pristine marine areas INP may originate from both oceanic sources and/or long range transport. Sampled aerosol particles ($PM_{10}$) were analysed for sodium and methanesulfonic acid (MSA). Resulting mass concentrations were used as tracers for primary marine and secondary aerosol particles, respectively. Sodium, with an average concentration around $2.8\,\mu\mathrm{g\,m}^{-3}$, was found to dominate the sampled particle mass. MSA was highly variable over the SO, with concentrations up to $0.5\,\mu\mathrm{g\,m}^{-3}$ near the sea ice edge. A correlation analysis yielded strong correlations between sodium mass concentration and particle number concentration in the coarse mode, unsurprisingly indicating a significant contribution of SSA to that mode. CCN number concentration was highly correlated with the number concentration of Aitken and accumulation mode particles. This, together with a lack of correlation between sodium mass and Aitken and accumulation mode number concentrations, underlines the important contribution of non-SSA, probably secondarily formed particles, to the

https://doi.org/10.5194/acp-2021-700
Preprint. Discussion started: 6 September 2021


Atmospheric Chemistry and Physics Discussions

CCN population. INP number concentrations did not significantly correlate with any other measured aerosol physico-chemical parameter.

## 1 Introduction

Earth's changing climate and the human influence on it are undeniable facts (IPCC, 2013). Emissions of greenhouse gases (e.g., carbon dioxide) and their impact on the radiation budget are well understood, with high confidence and low uncertainty. A larger uncertainty emerges from the lack of knowledge on atmospheric aerosol particles, in particular their influence on cloud-radiative properties. As there are natural and anthropogenic aerosol sources, the human impact on aerosol-cloud interactions is difficult to quantify. One way of reducing the uncertainty concerning the human influence on atmospheric aerosol particles, pointed out by Carslaw et al. (2013), is better constraining conditions before human impact, in the preindustrial time. With an atmospheric general-circulation model, Hamilton et al. (2014) searched for still-existing regions with preindustrial-like conditions, by comparing simulations of atmospheric conditions in 1750 and 2000. The Southern Ocean region was found to feature pristine aerosol conditions during the Southern hemisphere summer months, making it an excellent region for measurements of pristine aerosol conditions. This was one of the key motivations for the "Study of Preindustrial-like Aerosol Climate Effects" (ACE-SPACE; Schmale et al., 2019) project within the framework of the Antarctic Circumnavigation Expedition (ACE), which was conducted across all sectors of the SO in the Austral summer 2016/17.

The focus of this study is on aerosol particles that can modulate cloud micro-physical properties and hence affect the cloud albedo (Twomey, 1974) and lifetime (Albrecht, 1989). Aerosol particles can initiate cloud droplet formation at levels of supersaturation ($SS$) much lower than the supersaturation necessary for homogeneous droplet formation (Köhler, 1936). The $SS$ at which particles activate is dictated primarily by their size, but also their chemical composition (Dusek et al., 2006). If a particle is a suitable condensation nucleus at atmospheric supersaturation conditions, it is called a cloud condensation nuclei (CCN). Another group of cloud property-altering aerosol particles are ice nucleating particles (INP), which initiate cloud droplet freezing above the point of homogeneous freezing at $-38\,^{\circ}\mathrm{C}$. In summary, CCN play an important role in the formation of clouds, while INP alter the phase state (frozen or liquid) of cloud droplets which affects cloud radiative properties (Vergara-Temprado et al., 2018). Furthermore, cloud glaciation influences the precipitation formation (Wegener, 1911) and dissipation of clouds (Albrecht, 1989). As a consequence, changes in cloud radiative properties and cloud lifetime impact Earth's climate (Lindzen, 1990; Murray et al., 2012). With that, CCN and INP play an important role in the current state of the atmosphere and observations are fundamental to estimate the progression of climate change.

Of the few aerosol-related studies over the SO, the majority focused on physical aerosol particle properties and aerosol composition. During the first Aerosol Characterization Experiment (ACE-1) in the Australian sector of the SO in 1995, Quinn et al. (1998) found the marine boundary layer (MBL) aerosol population with a particle diameter ($D_\mathrm{p}$) between $100$ and $300\,\mathrm{nm}$ (referred to as "accumulation mode") to be minimally influenced by sea salt and mainly comprised of non-sea salt (nss) sulfate, i.e. the fraction of total sulfate not associated with sea salt. The main sources of nss-sulfate are: 1. sulfur compounds derived from continental anthropogenic sources (Savoie and Prospero, 1989), 2. oxidation of atmospheric dimethyl sulphide (DMS)

https://doi.org/10.5194/acp-2021-700
Preprint. Discussion started: 6 September 2021


Atmospheric Chemistry and Physics Discussions

(Covert et al., 1992; Raes, 1995), and 3. volcanic emissions. DMS is produced by marine microbial activity and emitted from the ocean into the atmosphere in the gas phase (Curran et al., 2003; Abram et al., 2010). Sulfate formation from DMS oxidation is a complex multi-step process involving several intermediate molecules. For the sake of brevity, we simplify the description of the processes with three main pathways: 1. sulfuric acid production from homogeneous gas phase oxidation followed by condensation, 2. sulfur dioxide production from homogeneous gas phase oxidation followed by heterogeneous oxidation in the liquid phase, and 3. reactive uptake on droplets or liquid particles followed by heterogeneous oxidation (Chen et al., 2018).

Properties of Aitken ($D_\mathrm{p} = 10$–$100\,\mathrm{nm}$) and accumulation mode particles ($D_\mathrm{p} = 100$–$1000\,\mathrm{nm}$ in this study) in the SO region were found to be clearly dependent on air mass origin, with two distinct air masses (polar and maritime) being encountered during the British Southern Ocean (BSO) campaign (O'Dowd et al., 1997), and the Plankton-derived Emissions of trace Gases and Aerosols in the Southern Ocean (PEGASO) cruise (Dall'Osto et al., 2017; Fossum et al., 2018). The two air masses featured distinctly different aerosol populations in terms of concentration and chemical composition. Looking at the composition of the larger particle size ranges, for ACE-1 the population of particles with $D_\mathrm{p} = 300$–$5000\,\mathrm{nm}$ (referred to as "coarse mode") was found to be dominated by sea salt, with sporadic and minor contributions from nss-sulfate. Variations in the coarse mode sea salt concentrations could only partially ($40\,\%$) be explained by local wind speeds (Quinn et al., 1998).

The concentrations of particles in the MBL of the SO that act as CCN were investigated by a smaller number of studies. Quinn et al. (2017) found a large portion of the Aitken mode to act as CCN at a $SS > 0.5\,\%$. Sea spray aerosol (SSA), a mix of sea salt particles and ocean-derived organic species (de Leeuw et al., 2011), was found to dominate the CCN population, but only at $SS = 0.1\,\%$ in the high latitudes (down to $70^\circ$ S) of the Southern hemisphere (Quinn et al., 2017). Cases of polar air during PEGASO featured CCN number concentrations at $SS = 0.8\,\%$ ($N_{\mathrm{CCN},0.8}$) of $217 \pm 31\,\mathrm{cm}^{-3}$, while maritime cases showed almost doubled concentrations ($420 \pm 168\,\mathrm{cm}^{-3}$).

It remains an open question how CCN abundance is distributed over the SO and what typical values are, especially during the pristine conditions of the Austral summer. Further, CCN properties and origin are of interest. It is know that new particle formation (NPF) in the free troposphere is an important source of CCN in the MBL and occurs frequently over the summertime SO (McCoy et al., 2021). To our knowledge, it is not known which process/source (e.g., NPF or SSA) governs the CCN population of the SO generally and what role horizontal and vertical atmospheric transport plays.

Studies of INP number concentration ($N_\mathrm{INP}$) and origin in the SO region started with immersion freezing experiments by Bigg (1973), who measured $N_\mathrm{INP}$ between 3–$250\,\mathrm{m}^{-3}$ at $-15^\circ$C. Two recent cruises: the Cloud, Aerosols, Precipitation, Radiation and Atmospheric Composition campaign (CAPRICORN I & II), observed $N_\mathrm{INP}$ over the SO in the temperature range between $-12$ and $-31^\circ$C varying between $0.04$ and $1000\,\mathrm{m}^{-3}$ (McCluskey et al., 2018). For context, $N_\mathrm{INP}$ at $-20^\circ$C was found to be lower by a factor of up to $100$ compared to Bigg (1973). They also investigated the contribution of biological INP using heat treatment methods, assuming biological INP to be heat-labile. McCluskey et al. (2018) found INP on the SO to be mainly heat-resistant, with contributions from heat-labile INP in the $-15$ to $-20^\circ$C temperature range. In Bigg (1973) it was hypothesised, based on the fact that INP concentrations did not increase significantly in the vicinity of Australia, that there was no influence of dust from the continent. Correlation of INP and ambient radon concentration was used to assess whether sampled INP have terrestrial or oceanic sources for both CAPRICORN cruises. The INP source potential of bubble

https://doi.org/10.5194/acp-2021-700
Preprint. Discussion started: 6 September 2021


Atmospheric Chemistry and Physics Discussions

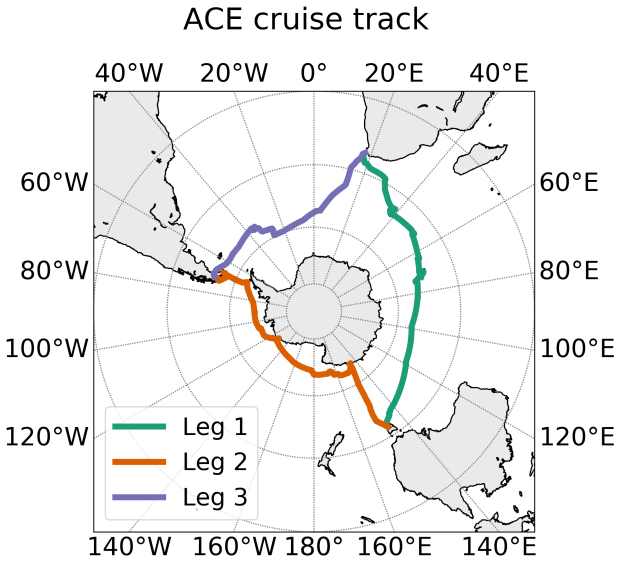


**Figure 1.** Hourly position of the RV *Akademik Tryoshnikov* during ACE. Leg 1 (green) from Cape Town (South Africa) to Hobart (Australia) between 20 December 2016 and 19 January 2017, Leg 2 (orange) from Hobart to Punta Arenas (Chile) between 22 January and 22 February 2017, and Leg 3 (purple) from Punta Arenas to Cape Town between 26 February and 19 March 2017.

bursting was characterised for CAPRICORN II in McCluskey et al. (2018), using seawater samples. They found that INP were from oceanic sources, aerosolized by bubble bursting. Additionally, Uetake et al. (2020) show that bacteria sampled during CAPRICORN II are mostly of marine origin, suggesting a restricted meridional transport of continental aerosol towards the SO. In consequence, a dominance of sea spray on INP was concluded.

However, data on INP abundance, spatial distribution, properties, and sources over the SO region remain sparse. Regayre et al. (2020) pointed out that already a small number of observations from the SO can effectively reduce model uncertainty more than hundreds of measurements in the Northern hemisphere, as current simulations are based on very few observations in the Southern hemisphere. This demonstrates a need for further field measurements of CCN and INP in the SO region.

In this study, we present circum-Antarctic measurements from three months of continuous on-line CCN measurements and filter sampling with subsequent INP, sodium and MSA analysis. Based on a correlation analysis, links between the measured properties are discussed.

## 2 Methods

Measurements were carried out in the framework of ACE (Walton and Thomas, 2018). The cruise took place between December 2016 and March 2017 on board the research vessel (RV) *Akademik Tryoshnikov*. Starting and ending in Cape Town (South Africa), the cruise was divided into three legs: Cape Town to Hobart (Australia), Hobart to Punta Arenas (Chile) and Punta Arenas to Cape Town (Fig. 1). Several islands (Marion, Crozet, Kerguelen, Balleny, Scott, Peter 1$^{st}$, Diego Ramierez, South

https://doi.org/10.5194/acp-2021-700
Preprint. Discussion started: 6 September 2021


Atmospheric Chemistry and Physics Discussions

Georgia, South Sandwich, and Bovetoya island), an Antarctic glacier (Mertz Glacier), and the Siple ice shelf were passed during ACE. At Mertz Glacier the southern-most latitude of 78° S was reached.

The instrumentation for real-time aerosol measurements was situated in a laboratory container on the fore-deck of the RV, equipped with two standard aerosol inlets (Global Atmosphere Watch; Weingartner et al., 1999) at roughly 15 m above sea level (a. s. l.), allowing for particles with $D_\mathrm{p} \leq 40\,\mu\mathrm{m}$ to be sampled. The sampled air was dried to a relative humidity below 40 %. An iso-kinetic splitter was used, together with as short as possible tubing, to feed the aerosol to the different instruments inside the measurement container.

The operated low- and high-volume filter samplers were positioned on the upper deck of the RV (∼28 m a. s. l.) and each one run on a $PM_{10}$ inlet. Further details on the filter sampling can be found in subsection 2.3. An ultrasonic anemometer was operated next to the high-volume filter sampler and provided wind direction data for an automatic shut-down mechanism for the high-volume sampler. Sampling was stopped automatically during periods with wind direction within a 180° half-circle at the sampler, with the RV's exhaust at 90°. A detailed description of the instrument set-up of the ACE-SPACE project is given in Schmale et al. (2019), and a full description of the instrument set-up during ACE is given in the cruise report by Walton and Thomas (2018). In the following, we focus on the instruments used in conjunction with our CCN- and INP-related investigations.

### 2.1 Aerosol Size Distribution

Particle number size distributions (PNSD) of aerosol particles in the mobility diameter range of 11–400 nm and aerodynamic range of 500 nm–19 µm were measured using a Scanning Mobility Particle Sizer (SMPS, custom-built by PSI) and an Aerodynamic Particle Sizer (APS, model 3321 by TSI inc., Shoreview, MN, USA), respectively. The custom-built SMPS instrument is further described in Wiedensohler et al. (2012). Validation of sizing accuracy of both instruments was performed using polystyrene latex spheres. To minimize influences of the ship exhaust, data filtering was performed for the SMPS and APS data, based on sudden changes in the total aerosol particle number concentration, concentrations of carbon dioxide, black carbon, and wind direction (Moallemi et al., 2021).

PNSD of SMPS and APS were merged by assuming spherical particle shape for the SMPS output to convert mobility diameter to geometric diameter as a first step. As a second step, the APS output is converted from aerodynamic to geometric diameter assuming spherical shape and material density of $1.8\,\mathrm{g\,cm^{-3}}$. The combination of both outputs enables interpolation of the gap between the SMPS ($D_\mathrm{p} \leq 400\,\mathrm{nm}$) and APS ($D_\mathrm{p} > 500\,\mathrm{nm}$) instruments. Further, a mode fitting technique analogue to Modini et al. (2015) was applied, that is based on a method described in Khlystov et al. (2004) and fully described in the supplement to Landwehr et al. (2021). Thereby, each PNSD is assumed to be a superposition of up to three aerosol modes and log-normal distributions in pre-defined size ranges are fitted. The three modes are Aitken (modal diameter in the range 1 to 20 nm; referred to as "mode 1" in the following), accumulation (10 to 100 nm; "mode 2"), and a sea-spray mode (centered around 140 to 220 nm; "mode 3"). For each time step, combining all fitted modes results in a smoothed total PNSD that is used where a measured PNSD is too noisy at low concentrations, e.g., for the calculation of the particle hygroscopicity parameter described in subsection 2.2. An example of the mode fitting is given in Fig. S1. Integration of smoothed total PNSD

https://doi.org/10.5194/acp-2021-700
Preprint. Discussion started: 6 September 2021


Atmospheric Chemistry and Physics Discussions

over all mobility diameters gave total aerosol particle number concentration ($N_{\mathrm{total}}$) for each time step. Analogously, the concentration of particles with $D_{\mathrm{p}} > 500\,\mathrm{nm}$ ($N_{500}$) was derived, which is later used in a commonly-used parameterization for INP concentration (see subsection 3.4).

### 2.2 Cloud Condensation Nuclei

A Cloud Condensation Nuclei counter (CCNc; *CCN-100* instrument by DMT, Boulder, CO, USA) was used to measure the CCN concentration at various $SS$. The CCNc's main part is a continuous-flow thermal gradient diffusion chamber, in which a stream-wise temperature gradient is induced to achieve defined $SS$ and corresponding particle activation to droplets. The aerosol flow rate inside the CCNc is $0.5\,\mathrm{L\,min^{-1}}$. Activated particles are counted by an optical particle counter. Further documentation on the CCNc can be found in Roberts and Nenes (2005). Calibration of the CCNc was performed prior to the cruise, following the standard operating procedure given in Gysel and Stratmann (2014) and recommendations in Schmale et al. (2017). During ACE, the CCNc was operated at $SS$ of 0.1, 0.15, 0.2, 0.3, 0.5, and 1 % maintained for ten minutes each. To ensure stable thermal conditions within the instrument, data collected during the first five minutes of each $SS$ set-point were discarded. Furthermore it was ensured that (1) the instrument's internal thermal stability control reported thermally stable conditions, and (2) the absolute difference between set and read temperature of the optics was smaller than 2 K. The remaining data were aggregated into one minute intervals and filtered for ship exhaust influences (same as for the SMPS and APS instruments). Based on the filtered values, averaged $N_{\mathrm{CCN}}$ at a particular $SS$ were calculated. This procedure results in one $N_{\mathrm{CCN}}$ value per hour and supersaturation. During data analysis, CCN concentrations at 0.1 % were found to lack sufficient data quality, therefore measurements at this supersaturation were discarded.

For determining the critical dry diameters for particle activation ($D_{\mathrm{crit}}$) and aerosol particle hygroscopicity parameters ($\kappa$), we applied the procedure used in, e.g., Kristensen et al. (2016) and Petters and Kreidenweis (2007). $D_{\mathrm{crit}}$ is implicitly defined as the lower boundary of the integral over the PNSD for which the integrated particle number concentration equals the measured CCN number concentration. In our case, the upper boundary of the integral was always $10\,\mu\mathrm{m}$, due to using instruments operated on a $\mathrm{PM}_{10}$ inlet. The $\kappa$ value, an indirect measure of chemical composition of the CCN at given $D_{\mathrm{crit}}$, is derived from the $SS$ applied in the CCNc and the corresponding $D_{\mathrm{crit}}$. Corresponding to $N_{\mathrm{CCN}}$, one $\kappa$ value per hour and supersaturation is determined. A Monte Carlo simulation (MCS) approach with an iterative solver was used, following the procedure described in Herenz et al. (2019), to model error propagation in both derivation of $D_{\mathrm{crit}}$ and calculation of $\kappa(D_{\mathrm{crit}})$. The calculation of $D_{\mathrm{crit}}$ and thus $\kappa$ is highly sensitive to the PNSD which, in our case, depends on the quality of the mode-fitting. To exclude unreasonable values, $D_{\mathrm{crit}}$ values were filtered. For this, the range between $10^{\mathrm{th}}$ and $90^{\mathrm{th}}$ percentile of $D_{\mathrm{crit}}$ was calculated for each $SS$ separately. $D_{\mathrm{crit}}$ values outside this range and associated $\kappa$ values were excluded from further analysis. Hence, the presented results are representative of the most frequently occurring $\kappa$ values.

### 2.3 Filter sampling for INP, sodium and MSA analysis

Filter sampling of ambient air for off-line INP, sodium and MSA analysis at the laboratories of Leibniz Institute for Tropospheric Research (TROPOS) was carried out using a high-volume sampler (HV; *DHA-80* filter sampler, DIGITEL, Volketswil,

https://doi.org/10.5194/acp-2021-700
Preprint. Discussion started: 6 September 2021


Atmospheric Chemistry and Physics Discussions

Switzerland). Further, a low-volume sampler (LV; *DPA-14* filter sampler, DIGITEL) was used to collect additional samples for INP analysis. LV sampling was performed at eight hours time resolution using track-etched polycarbonate membrane filters (Whatman Nuclepore, Cytiva, Little Chalfont, UK; $200\,\mathrm{nm}$ pore size, $47\,\mathrm{mm}$ in diameter) at a flow rate of roughly $25\,\mathrm{L\,min^{-1}}$. The HV sampler used a flow rate of roughly $500\,\mathrm{L\,min^{-1}}$, sampling air through quartz-fibre filters (*MK 360*, Munktell, Bärenstein, Germany) of $150\,\mathrm{mm}$ in diameter for up to 24 hours per filter. Here, each filter's individual sampling time ($<1$ to $1437\,\mathrm{min}$) was dependent on the automatic shut-down mechanism. In total, 258 LV and 94 HV filters were collected throughout the cruise, including five (four) un-sampled reference filters for LV (HV) sampling, called field blank filters (FBF). FBF were handled in the same way as the sampled ones, enabling assessment of background concentrations due to both methodology and handling. After sampling, filters were stored in a freezer at $-20^{\circ}\mathrm{C}$ and shipped frozen to TROPOS for offline analysis after the cruise concluded. INP analysis was performed for both LV and HV filters. LV filters were used solely for the INP analysis, while the HV filters were split between INP, sodium and MSA analysis and reserve samples. HV filters with a too small sampling volume ($<100\,\mathrm{m^3}$), due to the aforementioned automated shut-down mechanism, were not considered further to prevent unreasonably high conversion factors to infer atmospheric concentrations from filter analysis results. A total of 79 sampled HV filters were included in the following analysis.

The freezing behaviour of the aerosol particles collected on each LV and HV filter was investigated using the Ice Nucleation Droplet Array (INDA) at TROPOS. INDA is based on the freezing array method described in Conen et al. (2012) and a detailed instrument description is given in the supporting information in Hartmann et al. (2019). As a first step of the analysis process, stored filters were acclimatised to roughly $-3^{\circ}\mathrm{C}$ in a fridge. LV filter contents were washed off by submerging the filter in $7.5\,\mathrm{mL}$ ($V_{\mathrm{water}}$; $10\,\mathrm{mL}$ at later stages) ultra-pure water (milliQ, $18.2\,\mathrm{M\Omega\,cm^{-2}}$). In contrast, 96 randomly punched-out pieces of $1\,\mathrm{mm}$ in diameter ($D_{\mathrm{punchout}}$) per filter were used for the INP analysis of the HV filters. The 96 wells of a PCR (polymerase chain reaction) plate (BRAND, Wertheim, Germany) were either filled with $50\,\mu\mathrm{L}$ each ($V_{\mathrm{droplet}}$) of the filter washing water (LV) or with $50\,\mu\mathrm{L}$ of milliQ water and one punch-out (HV). The PCR plate was sealed and partially submerged in the ethanol bath of a cryostat (*FP 40*, Julabo, Seelbach, Germany). Cooled at a rate of roughly $1\,\mathrm{K\,min^{-1}}$, the number of frozen droplets ($n_{\mathrm{frozen}}$) and corresponding temperature ($T$) was documented automatically every six seconds. Recommendations on sample handling and processing given in Polen et al. (2018) were followed.

The frozen fraction ($f_{\mathrm{ice}}$) was calculated by dividing $n_{\mathrm{frozen}}$ by the total number of droplets per PCR plate ($n_{\mathrm{total}} = 96$). Obtained $f_{\mathrm{ice}}$ at any $T$ was used to derive the cumulative INP concentration $N_{\mathrm{INP}}$, using:

$$N_{\mathrm{INP}}(T) = -\frac{ln(1 - f_{\mathrm{ice}}(T))}{V} \tag{1}$$

according to Vali (1971). The reference volume $V$ for the LV filters was calculated as:

$$V = \frac{V_{\mathrm{flow}}}{V_{\mathrm{water}}} * V_{\mathrm{droplet}}, \tag{2}$$

where $V_{\mathrm{flow}}$ is the sampled air volume, $V_{\mathrm{water}}$ is the volume of washing water and $V_{\mathrm{droplet}}$ is the water volume per PCR plate well. For the HV filters, $V$ was calculated using:

$$V = \frac{(0.5 * D_{\mathrm{punchout}})^2}{(0.5 * D_{\mathrm{filter,HV}})^2} * V_{\mathrm{flow}}, \tag{3}$$

https://doi.org/10.5194/acp-2021-700
Preprint. Discussion started: 6 September 2021


Atmospheric Chemistry and Physics Discussions

where $D_{\mathrm{punchout}}$ is the diameter of the filter sub-sample per well and $D_{\mathrm{filter,HV}}$ the diameter of a HV filter. $V_{\mathrm{flow}}$ was logged by both (LV and HV) samplers.

Uncertainties arising from the methodology were assessed similarly to previous studies (e.g., Wex et al., 2019; Gong et al., 2020). Confidence intervals for $f_{\mathrm{ice}}(T)$ of each filter were determined using a method described in Agresti and Coull (1998). Resulting lower and upper values of each $f_{\mathrm{ice}}(T)$ in Eq. 1 are reported as error bars of $N_{\mathrm{INP}}(T)$ values.

To provide data points from each filter at a given temperature, estimated INP concentrations are given for cases when ice fractions of $f_{\mathrm{ice}} = 0$ or $f_{\mathrm{ice}} = 1$ were obtained, i.e., none or all wells of the PCR plate were frozen. For these two cases, Eq. 1 is not applicable to calculate valid concentrations. We then assume the probabilities of either none ($f_{\mathrm{ice}} = 0/96$) or one ($f_{\mathrm{ice}} = 1/96$) of the PCR wells to be frozen as equal. A similar assumption is made when all ($f_{\mathrm{ice}} = 96/96$) or all but one ($f_{\mathrm{ice}} = 95/96$) wells are frozen. Considering $f_{\mathrm{ice}} = 1/96$ and $f_{\mathrm{ice}} = 95/96$ in Eq. 1 yields estimates for the lower and upper limit of detectable $N_{\mathrm{INP}}$, respectively.

Based on the $f_{\mathrm{ice}}$ of the FBF, we determined averaged temperature-dependent INP concentrations for the FBF ($N_{\mathrm{INP,FBF}}$), which were used as background $N_{\mathrm{INP}}$ for our sampled filters. Equation 1 with an average (mean $\pm$ SD) volume of sampled air for all sampled LV (HV) filters of $8.95 \pm 0.74\,\mathrm{m}^3$ ($471.3 \pm 151.4\,\mathrm{m}^3$) was used to calculate $N_{\mathrm{INP,FBF}}$. In Tab. S3 $N_{\mathrm{INP,FBF}}$ is given for the LV filters. No correction for contamination by the RV's stack exhaust was applied, as it was shown in Welti et al. (2020) that ship exhaust is not ice-active in the temperature range we are presenting ($T > -30\,^{\circ}\mathrm{C}$).

Analysis of the HV filters regarding mass concentrations of sodium and MSA was performed. Total filter load for each HV filter was determined using a micro-balance (*AT261 Delta Range*, Mettler Toledo, Greifensee, Switzerland). Filter contents were extracted and ion chromatography performed, following the procedures described in Müller et al. (2010) and van Pinxteren et al. (2017). Results of the analysis were corrected for standard conditions and are reported as atmospheric mass concentrations (in $\mu\mathrm{g\,m}^{-3}$). An influence from the RV's exhaust stack on the measured sodium or MSA concentrations is not expected due to their respective source mechanism. Sodium is used as a conservative tracer for primary aerosol particles of marine origin, and MSA was found to be solely a product of DMS oxidation (Legrand and Pasteur, 1998).

### 2.4 Further resources

During the ACE cruise sea water was sampled every four hours using the RV's underway water supply system and during CTD (conductivity, temperature and depth) rosette deployments, at specific depths up to $200\,\mathrm{m}$ (Walton and Thomas, 2018). Glass fibre filters ($25\,\mathrm{mm}$ in diameter, $700\,\mathrm{nm}$ pore size) were sampled with up to $2\,\mathrm{L}$ of sampled sea water under low vacuum pressure and stored at $-80\,^{\circ}\mathrm{C}$ prior to analysis on-board the RV. After extraction in $90\,\%$ acetone for $24\,\mathrm{h}$, chlorophyll a (Chl-*a*) pigment concentration (in $\mathrm{mg\,m}^{-3}$) was measured on a fluorometer (*AU-10*, Turner Designs, San Jose, CA, USA). Calibration was performed against a standard Chl-*a* solution (Sigma-Aldrich, St. Louis, MO, USA). Concentrations of volatile organic compounds (VOC), like isoprene and DMS, in sea water were measured using a gas chromatography-mass spectrometry system (*5975-T LTM-GC/MSL*, Agilent Technologies, Santa Clara, CA, USA) by the Surveying Organic Reactive gases and Particles Across the Surface Southern Ocean (SORPASSO) project. A description of the full procedure can be found in Rodriguez-Ros et al. (2020).

https://doi.org/10.5194/acp-2021-700
Preprint. Discussion started: 6 September 2021


Atmospheric Chemistry and Physics Discussions

Continuous data of wind speed and direction during the cruise were obtained from two ultrasonic anemometers (part of *MAWS 420* system, Vaisala, Vantaa, Finland) located on the port- and starboard side of the RV on the observation deck ($\sim$30 m a. s. l.) above the bridge of the RV (Walton and Thomas, 2018). Observed wind speeds were corrected by Landwehr et al. (2020). To estimate the wind speed at 10 m a. s. l. ($U_{10}$), measurement height and atmospheric stability were considered using a logarithmic wind speed profile, including the drag coefficient. Quantification of air-flow distortion bias generated by the RV's structures was performed using the data from the operational ERA-interim weather model as a free stream reference. The resulting correction was applied to the observed wind speed, leading to a data set of wind speed at 10 m a. s. l. for the cruise with a five minute time resolution.

The distance between the RV's position and the nearest land for ACE was calculated by Volpi et al. (2020) using the cruise track and additional information on islands in the SO inside a geographic information system application.

### 2.5 Correlation analysis

The collected data were used in a correlation analysis. The goal was to characterise the aerosol population on the SO by finding possible connections between their associated quantities, with the strength/lack of correlation as a first hint for potential sources.

Input variables were the MSA and sodium concentrations from the HV filters, INP concentrations at five temperatures ($-8$, $-12$, $-16$, $-20$, and $-24$°C) from the LV filters, $N_{\text{total}}$, $N_{500}$, particle concentrations of individual PNSD modes ($N_{\text{mode1}}$, $N_{\text{mode2}}$, and $N_{\text{mode3}}$), $N_{\text{CCN}}$ at all measured $SS$ and respective $\kappa$ values, wind speed at 10 m a. s. l. ($U_{10}$) and in-water Chl-*a* and DMS concentrations. Correlation analysis was performed by calculating Spearman's rank correlation coefficients and associated $p$ values between input variables. As data of diverse temporal resolution were used, the coarsest resolution (24 h, HV filter sampling) was chosen and variables with finer resolution were averaged over 24 hour periods, using arithmetic mean values. For each variable, 79 data points were used for the correlation analysis. This corresponds to the number of HV filters which sampled a sufficient ($>$100 m$^3$) volume (see subsection 2.3).

## 3 Results and Discussion

### 3.1 Aerosol Particles and Cloud Condensation Nuclei

In Fig. 2a, smoothed PNSD for legs 1–3 of ACE are presented. For the most parts of the cruise, a bi-modal particle number size distribution was present. Potential sources for the pronounced accumulation mode, which is causing the bi-modality, are either entrainment of aerosol particles from the free troposphere (FT) into the MBL or in-cloud processing, according to Hoppel et al. (1986). A general characterisation of the aerosol particles sampled during ACE is given in Schmale et al. (2019), including median values for the diameter of the Hoppel minimum, which are 48, 74, and 68 nm for Leg 1, Leg 2, and Leg 3, respectively (see Fig. 2a).

Time series of $N_{\text{total}}$ and $N_{\text{CCN}}(SS)$ for the ACE cruise are given in Fig. 2b. Here, days for which the average distance to land is lower than 200 km are highlighted with grey shading. Additionally, the starts and ends of the different cruise legs

https://doi.org/10.5194/acp-2021-700
Preprint. Discussion started: 6 September 2021


Atmospheric Chemistry and Physics Discussions

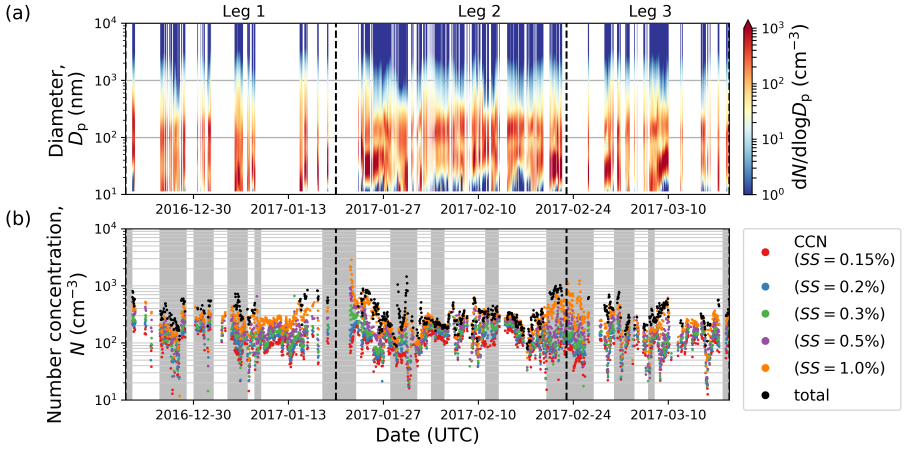


**Figure 2.** Time series of (a) hourly smoothed PNSD, and (b) total aerosol particle (black) and CCN number concentration (colour-coded by supersaturation) during legs 1–3. Ports visited (dotted lines) and vicinity to land (grey area) are indicated in the figure. Data gaps stem from filtering for instrument availability and exclusion of stack exhaust contamination periods. In (a) the Hoppel minimum can be seen as local minimum in the Aitken mode of the PNSD (Leg 1: 48 nm, Leg 2: 74 nm, Leg 3: 68 nm on average).

are given as dashed lines. Filtering by stack exhaust contamination caused concurrent data unavailability, while differences in temporal resolution and availability of the instruments create times with no overlap between $N_{\mathrm{total}}$ and $N_{\mathrm{CCN}}(SS)$. Fig. 2b shows that $N_{\mathrm{CCN}}$ at a particular $SS$ varied over 2 orders of magnitude throughout the cruise, e.g., at a $SS$ of 0.2 % ($N_{\mathrm{CCN,0.2}}$) from 4 to 309 cm$^{-3}$, which is consistent with the frequency distribution in Fig. 4a. In the vicinity of the ports, higher $N_{\mathrm{total}}$ and $N_{\mathrm{CCN}}(SS)$ are observed compared to the open ocean sections (stack exhaust contamination filtering being performed for both as described in subsection 2.2). This suggests aerosol particle abundance to be influenced by terrestrial and anthropogenic sources and is in line with Schmale et al. (2019) showing pristine conditions during ACE being encountered only south of 55° S.

Periodic differences between $N_{\mathrm{total}}$ and $N_{\mathrm{CCN,1.0}}$ throughout the cruise were observed (Fig. 2b). Periods of larger differences coincide with PNSD in Fig. 2a featuring a pronounced Aitken mode ($D_{\mathrm{p}} = 10$–$100$ nm) with elevated numbers in the size range below 40 nm. During these periods even $SS = 1$ % was not sufficient to activate the smaller Aitken mode particles. Consequently, quantities presented later in this manuscript, that are derived from $N_{\mathrm{CCN,1.0}}$, are representative for the larger Aitken mode particles, as $D_{\mathrm{crit}}$ at this $SS$ (∼37 nm, see Tab. S1) still falls within the Aitken mode.

In addition to the time series presented in Fig. 2b, spatial distribution of $N_{\mathrm{CCN}}$ at all measured $SS$ are given as daily averages in Fig. S2. Averages of $N_{\mathrm{CCN}}(SS)$, for the three legs of ACE are shown in Fig. 3a, individually. Due to the frequency distributions of $N_{\mathrm{CCN}}$ in Fig. 4a (introduced later) resembling log-normal distributions, leg-aggregated data and variability are given as geometric mean and geometric standard deviation values, respectively. $N_{\mathrm{CCN}}$ values increase with $SS$, e.g., for Leg 1 from 91 cm$^{-3}$ ($N_{\mathrm{CCN,0.15}}$) to 241 cm$^{-3}$ ($N_{\mathrm{CCN,1.0}}$). For all $SS$, the largest geometric mean values of $N_{\mathrm{CCN}}(SS)$ are observed during Leg 2. Moreover, the average Hoppel minimum diameter was found to be the largest for Leg 2, when compared to the

https://doi.org/10.5194/acp-2021-700
Preprint. Discussion started: 6 September 2021


Atmospheric Chemistry and Physics Discussions

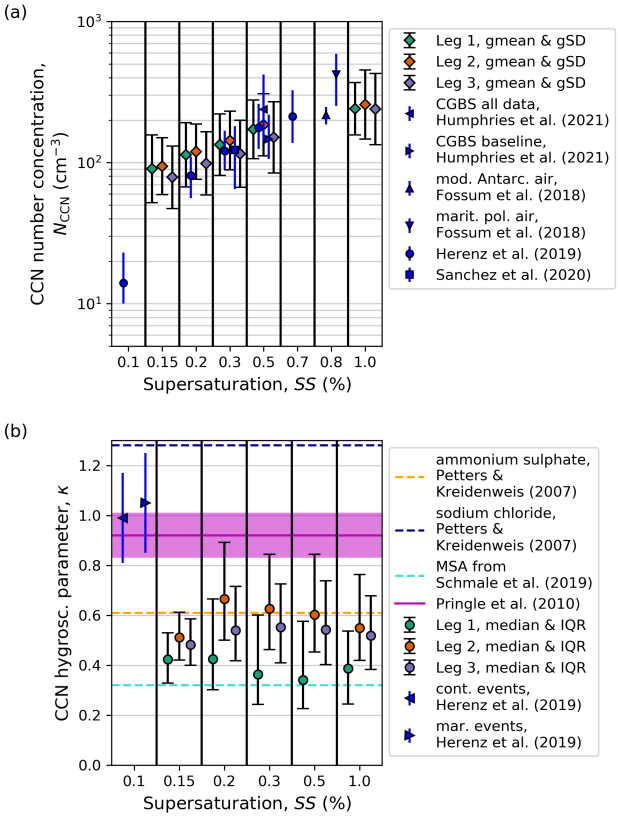


**Figure 3.** (a) Geometric mean values (gmean) and geometric standard deviation (gSD; whiskers) of CCN number concentration ($N_{\mathrm{CCN}}$) and (b) median values and respective inter-quartile range (IQR) of aerosol particle hygroscopicity parameter ($\kappa$). Both $N_{\mathrm{CCN}}$ and $\kappa$ are given as function of supersaturation ($SS$) for Leg 1 (green), Leg 2 (orange) and Leg 3 (purple), respectively. All $\kappa$ values resulting from $D_{\mathrm{crit}}$ values outside of $10^{\mathrm{th}}$ to $90^{\mathrm{th}}$ percentile range for $D_{\mathrm{crit}}$ (per $SS$) are excluded here. Included for comparison in (a) are the averages (median and IQR) over all measurements at CGBS coinciding with PEGASO and CAPRICORN-II from Humphries et al. (2021) (triangle left) and measurements for "baseline" conditions (triangle right) during that period. Baseline conditions are defined as wind directions between 190 and 280°, and ambient radon concentrations below $100\,\mathrm{mBq\,m^{-3}}$. Averages for events of modified Antarctic air (upward triangles) and maritime polar air (downward triangles) from Fossum et al. (2018) are given. As reference, mean $\kappa$ values for sodium chloride (dashed black line) and ammonium sulfate (dashed orange line) from Petters and Kreidenweis (2007), and a hypothetical $\kappa$ value for MSA from Schmale et al. (2019) (dashed teal line) are given in (b). Averages for Antarctica from Herenz et al. (2019) for cases of continental (triangles left) and marine events (triangles right) are given. Modelled $\kappa$ values for the Southern Ocean's surface layer (magenta line and area) from Pringle et al. (2010) for reference.

other two legs, indicating a pronounced Aitken mode. This, together with Schmale et al. (2019) showing less contribution (relative and absolute) of SSA to CCN during Leg 2, suggests a significant fraction of CCN originating from secondary aerosol production. However, differences in $N_{\mathrm{CCN}}$ between legs are within the ranges given by the respective geometric standard

https://doi.org/10.5194/acp-2021-700
Preprint. Discussion started: 6 September 2021


Atmospheric Chemistry and Physics Discussions

deviations. Therefore, the impact of longitudinal differences on CCN abundance is either small against the overall variability of the data, or a variety of effects cancel each other out so that no clear latitudinal trend can be observed. A similar conclusion can be drawn in terms of latitudinal trends, because the majority of the cruise track during Leg 2 was south of $60°$ S, compared to legs 1 and 3 being solely north of $60°$ S. With this, the CCN concentrations given in Tab. S1 can be considered representative for the whole SO region.

In addition to our data, $N_{CCN}$ from a selection of other studies performed on Antarctica or over the SO are given in Fig. 3a. For the continental Antarctic research station *Princess Elisabeth* (PES), located at $71.95°$ S and $23.35°$ E on East Antarctica's Queen Maud Land and about $200\,km$ in-land from the Antarctic coast, Herenz et al. (2019) reported $N_{CCN,0.1}$, $N_{CCN,0.2}$, $N_{CCN,0.3}$, $N_{CCN,0.5}$, and $N_{CCN,0.7}$. Overall, we find good agreement between values for the measurement period 2013–2016 in Herenz et al. (2019) and the geometric mean values of this study covering roughly three months during the Austral summer. The reported concentrations of $N_{CCN,0.2}$, $N_{CCN,0.3}$, and $N_{CCN,0.5}$ for cases of maritime air masses reaching PES show a difference of $-28\,\%$, $-9\,\%$, $+3\,\%$ to our values, respectively. Differences are expected, since (1) the station is not located directly at the Antarctic coast and (2) the number of measurements during the Austral summer is higher (three years). A better agreement at higher $SS$ suggests that differences arise from larger particles, that in general activate at lower $SS$. At the Australian Cape Grim Baseline Station (CGBS; $40.68°$ S, $144.68°$ E), $N_{CCN,0.5}$ is measured continuously since the mid-1970s (Gras and Keywood, 2017). In Humphries et al. (2021), average $N_{CCN,0.5}$ over the time frame November 2017 to March 2018 for CGBS are given. For the whole period, a median of $\sim 230\,cm^{-3}$ is reported (triangle left in Fig. 3a). This is above our average (mean $\pm$ SD) of $189 \pm 76\,cm^{-3}$ for Leg 1 and differences could be due to continental air masses reaching CGBS. Conditions at CGBS are only representative for the SO when the wind direction is between $190°$ and $280°$, the so-called "baseline" conditions (Gras and Keywood, 2017). The ambient radon concentration is used as a proxy for terrestrial influence (e.g., McCluskey et al., 2018) and a threshold of $100\,mBq\,m^{-3}$ is used in Humphries et al. (2021). By excluding measurements at CGBS that are not from baseline conditions, a median of $\sim 130\,cm^{-3}$ (triangle right in Fig. 3) can be found. This is in good agreement with our results for Leg 1 and we conclude that the terrestrial influence on our average values is small. As for ship-based CCN measurements, comparison between our findings and the PEGASO cruise in the SO's Atlantic sector during January–February 2015 (Fossum et al., 2018) can only be done semi-quantitatively, since $SS$ are not identical. Further, a comparison is only reasonable for Leg 3, the part of ACE on the Atlantic sector of the SO. The result of visual interpolation between our $N_{CCN,0.5}$ and $N_{CCN,1.0}$ for Leg 3 lies in the ranges of $217 \pm 31\,cm^{-3}$ reported for modified Antarctic air encountered during PEGASO (Fig. 3a). For the BSO cruise, only CCN concentrations inferred from nss-sulfate are available in O'Dowd et al. (1997), not comparable with any of our $N_{CCN}$. As for aircraft-based CCN measurements, $N_{CCN,0.3}$ between 17 and $264\,cm^{-3}$, with an average of $123 \pm 58\,cm^{-3}$ (mean $\pm$ SD), are report in Sanchez et al. (2021) for flights through the MBL between 42.5–$62.1°$ S and 133.8–$163.1°$ E during the Southern Ocean Clouds, Radiation, Aerosol Transport Experimental Study (SOCRATES). The reported concentrations are slightly lower than what was measured in that area during ACE, with values between 48 and $452\,cm^{-3}$ and an average of $178 \pm 99\,cm^{-3}$ (mean $\pm$ SD). Besides the difference in measurement height (SOCRATES: $50\,m$ a. s. l. until height of inversion; ACE: $\sim 15\,m$ a. s. l., see section 2), another factor is that measurements are from successive years, with the

https://doi.org/10.5194/acp-2021-700
Preprint. Discussion started: 6 September 2021


Atmospheric Chemistry and Physics Discussions

ACE cruise being in that area during 16 January to 26 January 2017 and the 15 flights during SOCRATES in the period of 15 January to 25 February 2018.

An overview on the aerosol particle hygroscopicity parameter $\kappa$ values observed during legs 1–3, individually, is given in Fig. 3b. Leg-wise averages of the hourly available $\kappa$ values per $SS$ are given as median values and respective inter-quartile ranges (IQR) because the frequency distributions of $\kappa(SS)$ in Fig. 4b (introduced later) do not resemble log-normal distributions. Error bars include both natural variability and the measurement uncertainty in $\kappa$, as described in subsection 2.2. Median $\kappa$ values for all legs and $SS$ are spread between $0.3$ and $0.7$, with a combined variability-uncertainty range (indicated by IQR as error bars) ranging from $0.2$ to $0.9$. Differences between legs can be seen, with the highest median values at each $SS$ found for Leg 2. Reference values for pure compounds or compound classes are given in Petters and Kreidenweis (2007), a mean $\kappa$ between $0.1$ and $0.2$ for organic material, $\kappa_{\mathrm{mean}} = 0.6$ for ammonium sulfate, $\kappa_{\mathrm{mean}} = 0.9$ for sulfuric acid, and $\kappa_{\mathrm{mean}} = 1.3$ for sodium chloride is reported. A typical $\kappa$ value for ammonium nitrate is omitted in Fig. 3b, as nitrate-containing compounds were found to not play an important role for the CCN population. Additionally, in Schmale et al. (2019) a $\kappa \sim 0.3$ for MSA is hypothesised. The majority of our $\kappa$ are above what is given for organic material and below the value given for sulfuric acid, which indicates that the sampled CCN population consists of a variable mixture of organic and inorganic materials. Median $\kappa$ values for Leg 1 are closest to what is assumed for MSA, while median values for leg 2 and 3 are closer to the value for pure ammonium sulfate. Looking at size-dependency, no clear trend of $\kappa$ between different $SS$ is apparent when considering error bars. For the size range between roughly 37 and $123\,\mathrm{nm}$ probed with our $SS$ (Tab. S1), this suggests the chemical composition to be independent of particle size, which further suggests a well-mixed aerosol (or CCN) population. However, when considering median values alone, for $SS > 0.15\,\%$ a slight decrease in $\kappa$ values with increasing $SS$ can be seen for Leg 2. Lower $\kappa$ values at higher $SS$ are in line with condensable organic vapors contributing to the aerosol chemical composition, while larger, aged particles activating at lower $SS$, are associated with higher $\kappa$ (McFiggans et al., 2006). Legs 1 and 3 do not feature increasing $\kappa$ values with decreasing $SS$, which suggests an internally mixed CCN population.

Comparison to Herenz et al. (2019) shows that our $\kappa$ values observed over the SO are much lower than the ones reported for the Austral summer on continental Antarctica, where $\kappa$ values at $SS = 0.1\,\%$ were found to be in the range between $0.8$ and $1.3$. This suggests significantly different particle composition at PES compared to the SO. Herenz et al. (2019) interpreted their sampled particles to be of mostly inorganic nature (i.e., sea spray) and therefore assumed a primary, marine origin. Our values, because of the overall small $\kappa$ values, hint towards a composition dominated by organics. Note, that particle sizes between 37 and $123\,\mathrm{nm}$ were probed with the $SS$ range of our instrument, hinting on the encountered aerosol population being mainly comprised of smaller particles. For SOCRATES, Saliba et al. (2020) report $\kappa$ values between $0.2$ and $0.5$ for particles with $D_{\mathrm{p}} < 100\,\mathrm{nm}$. Our $\kappa$ values in this size range (corresponding to $SS > 0.2\,\%$) lie partially in a similar range (Leg 1) and partially on the upper end (legs 2 and 3) of the range found during SOCRATES, respectively.

Using a global numerical weather model, simulations of $\kappa$ at $SS = 0.1\,\%$ for the SO region were presented in Pringle et al. (2010). Model results give values of $0.9 \pm 0.1$ for the surface layer. Comparison to our results suggests an overestimation of sea salt contribution and/or an underestimation of the presence of organic material in the model. A similar effect is noted in Schmale et al. (2019), when the $N_{\mathrm{CCN},0.2}$ measured during ACE are compared to the output of the Global Model of Aerosol

https://doi.org/10.5194/acp-2021-700
Preprint. Discussion started: 6 September 2021


Atmospheric Chemistry and Physics Discussions

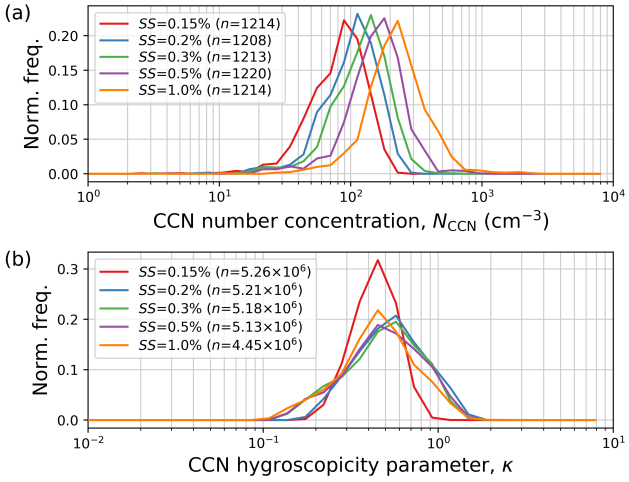


**Figure 4.** Normalized probability density function of (a) CCN number concentration $N_{\mathrm{CCN}}$ and (b) hygroscopicity parameter $\kappa$ for levels of supersaturation 0.15, 0.2, 0.3, 0.5, and 1 % (colour-coded) for legs 1–3. $N_{\mathrm{CCN}}$ values were measured at a five minute resolution. $\kappa$ values result from Monte-Carlo simulation runs ($n_{\mathrm{MCS}} = 10^4$) of hourly smoothed PNSD. $\kappa$ values that resulted from $D_{\mathrm{crit}}$ outside of $10^{\mathrm{th}}$ to $90^{\mathrm{th}}$ percentile range (per $SS$) are excluded. The number of data points is indicated ($n$).

Processes (GLOMAP) model. The largest differences between measurements and model output coincided with the highest gaseous MSA concentrations, suggesting an underestimation of CCN from secondary origin. A global model producing $\kappa$ values for the SO region twice as high compared to what we measured in situ reveals a strong discrepancy in CCN properties and the modelled CCN interacting with clouds.

Geometric mean values (and respective geometric standard deviation) of $N_{\mathrm{CCN}}$ and $D_{\mathrm{crit}}$, and median values (and respective IQR) of $\kappa$ for the entire cruise and its three legs are summarized in Tab. S1.

Probability density functions (PDF) of normalized frequencies for $N_{\mathrm{CCN}}(SS)$ and $\kappa(SS)$ during legs 1-3 are given in Fig. 4. PDF of $N_{\mathrm{CCN}}$ (Fig. 4a) show mono-modal distributions for all $SS$, with the PDF maxima shifting towards higher $N_{\mathrm{CCN}}$ with increasing $SS$, e.g., $\sim$90 cm$^{-3}$ at 0.15 % to $\sim$210 cm$^{-3}$ at 1 %. Comparing the distribution for $N_{\mathrm{CCN},0.2}$ (blue line in Fig. 4a) with yearly-averaged PDF from measurement sites around the globe in Schmale et al. (2018), our values show lower number concentrations with a PDF maximum at $\sim$100 cm$^{-3}$ and share resemblance in terms of number of modes and maximum location with the distribution reported for clean marine conditions (mono-modal, maximum at $\sim$200 cm$^{-3}$). For the MBL legs of SOCRATES, the PDF for $N_{\mathrm{CCN},0.3}$ is bi-modal, with peaks at 100 and 150 cm$^{-3}$ (Sanchez et al., 2021).

A change in distribution shape with increasing $SS$ can be seen for PDF of $\kappa(SS)$ in Fig. 4b. All five shown distributions have their maximum between 0.4 and 0.6, while a mono-modal distribution is only found for $\kappa_{0.15}$ (red line). PDF for $SS$ of 0.3, 0.5, and 1 % (green, purple, and orange line, respectively) feature a tail towards smaller values of $\kappa$, which could be interpreted as an additional mode. This occurrence of small particles (activated at high $SS$) consisting of mainly organic material forms a strong case for the sampled Aitken-mode CCN originating from secondary organic aerosol formation and growth processes.

https://doi.org/10.5194/acp-2021-700
Preprint. Discussion started: 6 September 2021


Atmospheric Chemistry and Physics Discussions

The accumulation mode, probed with the measurement at $SS = 0.15\,\%$, shows similar $\kappa$ values as the Aitken mode (Fig. 4b), while its $N_{\mathrm{CCN}}$ values are on average over $33\,\%$ smaller (Fig. 4a). Additionally, PDF for all $SS$ other than $0.15\,\%$ feature a tail towards higher $\kappa$ values. Such high $\kappa$ values at high $SS$ seem counter-intuitive and are indicative of highly hygroscopic Aitken mode particles being sampled. A sensitivity study of our methodology with respect to (1) modelling the measurement uncertainty via Monte Carlo simulations (Fig. S3a), (2) consideration of error propagation, and (3) quality of the fitted modes to the PNSD was performed. As $\kappa$ values were robust against these variations, we conclude that this tail (yet counter-intuitive) is not an artefact that stems from our methodology. However, to avoid speculation on the reason, we take a conservative approach in keeping the focus of the interpretation on the median values presented in Fig. 3b.

### 3.2 Ice Nucleating Particles

Time series of $N_{\mathrm{INP}}(T)$ for $T = -24^{\circ}\mathrm{C}$ ($N_{\mathrm{INP},-24}$; orange), $N_{\mathrm{INP},-20}$ (purple), $N_{\mathrm{INP},-16}$ (blue), $N_{\mathrm{INP},-12}$ (green), and $N_{\mathrm{INP},-8}$ (magenta) are given in Fig. 5a-e, respectively. Triangles indicate INP concentrations outside the detectable range, estimated as described in subsection 2.3. Measurement uncertainties (indicated by error bars) become smaller with decreasing temperature. This is due to (1) increased freezing probability with decreasing temperature, and (2) the measurement uncertainty being described by binomial sampling confidence intervals (following Agresti and Coull, 1998). The combination of both effects results in smaller error bars at lower temperatures. At $-12$ and $-16^{\circ}\mathrm{C}$, $N_{\mathrm{INP}}$ show the highest variability of around 3 orders of magnitude. At $-8$ and $-20^{\circ}\mathrm{C}$ the variability decreases to about two orders of magnitude, while $N_{\mathrm{INP}}$ at $-24^{\circ}\mathrm{C}$ only varies within 1 order of magnitude, because $N_{\mathrm{INP}}$ are close to and above the upper limit of detection. Each of the shown time series of $N_{\mathrm{INP}}$ in Fig. 5 contains episodes of elevated INP concentrations, coinciding with the RV being close to land (grey area) and harbours at the beginning of each leg (dashed line). During the open ocean sections of the cruise the majority of data points shows up to 2 orders of magnitude lower concentrations (e.g., $N_{\mathrm{INP},-16}$ of 0.1 to $10\,\mathrm{m}^{-3}$). This suggests that elevated atmospheric INP concentrations are connected to terrestrial (including coastal) INP sources. Without a tracer of terrestrial influence, e.g., measurements of ambient radon concentrations in McCluskey et al. (2018), assessment of air mass origin is not possible for ACE and the aforementioned connection remains without solid prove. A way of determining the parts of ACE on the open ocean is presented in Moallemi et al. (2021) using a threshold of $200\,\mathrm{km}$ in distance between the RV's position and the nearest land mass. However, this is only an approximation based on a higher unlikeliness of terrestrial signal away from land rather than looking at the actual air mass origin and thus not considered as a quantitative in this study. For comparison, Fig. 5c shows the range between the $5^{\mathrm{th}}$ and $95^{\mathrm{th}}$ percentile of $N_{\mathrm{INP},-15}$ from Bigg (1973) (orange area). They sampled filters on the SO around Australia, collecting 0.3 and $3\,\mathrm{m}^3$ of ambient air through a pair of membrane filters, respectively. In terms of sampling strategy, our LV sampling of $12\,\mathrm{m}^3$ through a porous filter over eight hours compares well with the sampling of Bigg (1973). The derivation of $N_{\mathrm{INP}}$ however was fundamentally different. In the supporting information (SI) of McCluskey et al. (2018), the effect of background INP concentrations during the study of Bigg (1973) is assessed and a correction proposed ($22\,\%$ lower values). This correction is applied to the values shown in Fig. 5c. The majority of our $N_{\mathrm{INP},-16}$ measurements are in the open ocean sectors and clearly below the range of $N_{\mathrm{INP},-15}$ observed by Bigg (1973). However, $N_{\mathrm{INP},-16}$ greater than $10\,\mathrm{m}^{-3}$ at the end of Leg 1, when the RV was in the vicinity of Australia, lie within the range of values from Bigg (1973).

https://doi.org/10.5194/acp-2021-700
Preprint. Discussion started: 6 September 2021


Atmospheric Chemistry and Physics Discussions

Our data are partially included in Welti et al. (2020) and form an integral part for a global view on marine INP concentrations. Spatial distributions of $N_{\mathrm{INP},-16}$ from our study and $N_{\mathrm{INP},-15}$ from Bigg (1973) are shown in Fig. S4c.

Average values of $N_{\mathrm{INP},-24}$, $N_{\mathrm{INP},-20}$, $N_{\mathrm{INP},-16}$, $N_{\mathrm{INP},-12}$ and $N_{\mathrm{INP},-8}$, sorted by legs of ACE, are given in Fig. 6. Values were determined including the estimates for maximum and minimum INP concentrations (triangles in Fig. 5). Differences in median values between different legs are largest at $-16\,^{\circ}\mathrm{C}$, while being within IQR. Mean values (crosses) are outside of the IQR for all temperatures other than $-24\,^{\circ}\mathrm{C}$.

A summary of average INP concentrations for legs 1–3 at selected temperatures is given in Tab. S2. Two different approaches were used for averaging using (a) only the values which are inside the detectable range or (b) including the values outside the detectable range by using a value on the edge of the detectable range instead (see subsection 2.3). Results of the two approaches differ in $N_{\mathrm{INP}}(T)$ mean, median, and geometric mean values by up to $\pm 50\,\%$. The largest differences were found for $N_{\mathrm{INP},-8}$ and $N_{\mathrm{INP},-24}$, where the number of data points outside the detectable range is highest. We report the average values with explicit reference to their potential biases.

PDF of $N_{\mathrm{INP}}$ at selected temperatures are shown in Fig. 7. $N_{\mathrm{INP}}(T)$ values outside of the detectable range are not considered for the PDF. Due to the overall small number of data points, the following discussion on PDF has to be considered as semi-quantitative. For the same reason, the PDF of $N_{\mathrm{INP},-8}$ is shown in Fig. 7e only for completeness and not discussed further. The $N_{\mathrm{INP},-12}$ and $N_{\mathrm{INP},-16}$ PDF (Fig. 7c,d) can be considered tri-modal. The lowest concentration mode in each of the two PDF exhibit values below $0.2\,\mathrm{m}^{-3}$ and contain values at the lower edge of the detectable range. Attributing these values to a particular source or origin is difficult. In Fig. 7c-e, averages for the upper and lower concentration limit are indicated (dashed line). The detection limit of individual measurements depends on the volume of sampled air and can be lower or higher than this average. The second, middle mode of $N_{\mathrm{INP},-12}$ and $N_{\mathrm{INP},-16}$ covers a range of higher concentration values (0.3 to $10\,\mathrm{m}^{-3}$ for $N_{\mathrm{INP},-16}$). Values in this range were encountered mainly during the open ocean sections of the cruise (Fig. 5c,d). As no further analysis on air mass origin was performed, we interpret this mode to contain a mix of typical marine signals, including marine sources and background concentration levels that could stem from long-range transport. In consequence, this mode is labeled "open ocean" (light blue area) in Fig. 7b-d. Moallemi et al. (2021) show that fluorescent primary biological aerosol particles (PBAP) measured during the open ocean sections of ACE originate mainly from SSA. With PBAP found to act as INP (e.g., Tobo et al., 2013), we conclude SSA to be a potential source for the INP we measured on the open ocean. The highest concentration mode in the PDF of $N_{\mathrm{INP},-12}$ and $N_{\mathrm{INP},-16}$ consists of values (e.g., 10 to $100\,\mathrm{m}^{-3}$ for $N_{\mathrm{INP},-16}$) measured close to land (see Fig. 5c,d). Hence, this mode is indicated as "Coastal" in Fig. 7b-d (yellow area). With our data, we cannot distinguish whether the sources of these INPs are located on the continents or the respective coastal regions. In Fig. 7c, a PDF of $N_{\mathrm{INP},-15}$ from Bigg (1973) is included (orange line). Here, only a subset of the total of 126 data points from Bigg (1973) is shown, containing the 58 data points south of $43^{\circ}\,\mathrm{S}$, mimicking the latitudinal range of the ACE cruise for a better comparison (Fig. S4). Differences between $N_{\mathrm{INP},-16}$ from this study and $N_{\mathrm{INP},-15}$ from Bigg (1973) are clearly visible, with over 1 order of magnitude lower maximum $N_{\mathrm{INP}}$ observed in our study. Agreement of their values is highest with the subset of our observations in the proximity to land.

https://doi.org/10.5194/acp-2021-700
Preprint. Discussion started: 6 September 2021


Atmospheric Chemistry and Physics Discussions

The PDF of $N_{\mathrm{INP},-20}$ is bi-modal (Fig. 7b), indicating contributions from terrestrial sources (higher concentration mode at 40 to 200 $\mathrm{m}^{-3}$). The lower concentration mode (1 to 40 $\mathrm{m}^{-3}$) represents the background concentrations from either terrestrial sources, and/or marine sources. A recent study (Cornwell et al., 2020) has shown that re-emission of dust particle from sea water into the atmosphere is possible and that the re-emitted particles retained their ability to act as INP. However, quantifying the contribution of this potential source is not possible with our data set.

The PDF of $N_{\mathrm{INP},-24}$ is mono-modal with a tail towards lower concentrations (Fig. 7a). We attribute this mono-modality foremost to the detectable range. Since the PDF represents a subset of the data ($n = 105$) with values that are not at the edge of the detectable range, a clear, elevated terrestrial and/or coastal signal can not be identified in the PDF. This interpretation is supported by the fact that the vast majority of $N_{\mathrm{INP},-24}$ measured close to land are above the detectable range (see Fig. 5a) and actual concentrations might be higher. In other words, the PDF given is representative for the marine environment. Note that INP active at this temperature range can be either of mineral nature and long-range transported from terrestrial sources, or originating from marine sources.

Welti et al. (2018) present PDF of $N_{\mathrm{INP}}(T)$ based on filters sampled at a fixed location on the Cabo Verde island of Sao Vicente, over a four year period (2009–2013). The PDF comprise changes in season, air mass origin, and bulk aerosol composition. The respective PDF of $N_{\mathrm{INP},-16}$, $N_{\mathrm{INP},-12}$, and $N_{\mathrm{INP},-8}$ are included for comparison in Fig. 7b-d. Welti et al. (2018) found log-normal distributions for all temperatures, and attributed them to random dilution during transport, indicating a lack of strong local sources. In other words, the PDF are thought to represent background INP concentrations at the Cabo Verde islands. Comparing PDF, it can be seen that for $N_{\mathrm{INP},-16}$ the bulk of our values is below what is reported in Welti et al. (2018), shifted by roughly 1 order of magnitude towards lower concentrations. For $N_{\mathrm{INP},-12}$ a respective shift is not as clearly seen, however a tendency towards more frequent occurrence of higher concentrations compared to our study is obvious. For $N_{\mathrm{INP},-8}$ this tendency is not visible anymore. The difference between the PDF given in Welti et al. (2018) and our study for $N_{\mathrm{INP},-12}$ and $N_{\mathrm{INP},-16}$ illustrate the latitudinal difference in marine $N_{\mathrm{INP}}$ with lower concentrations in the SO compared to the Atlantic.

The temperature spectra of $N_{\mathrm{INP}}$ for all filters sampled during ACE are given in Fig. 8. The highest freezing onset was found at $-4$°C. Between filters, $N_{\mathrm{INP}}$ is spread over up to 3 orders of magnitude at individual temperatures. This mirrors what can be seen in the PDF in Fig. 7 and indicates the frequent absence of local sources and the importance of long-range transport and related dilution processes for the prevailing INP concentrations. In the range of $-12.5$ to $-22.5$°C, only the lowest curves of our spectra lie within the range observed by McCluskey et al. (2018), who observe even lower $N_{\mathrm{INP}}$ in the SO. Differences in sampled geographical area (roughly 43–53° S and 141–151° E; this study: 34–78° S, circum-Antarctic) and season (March–April; this study: December–March) could be reasons for the observed differences.

Additional INP spectra determined from HV samples (*DHA-80* sampler, see subsection 2.3) are given in Fig. S5. Compared to the LV results in Fig. 8, the determined $N_{\mathrm{INP}}(T)$ are higher and in a narrower range. LV and HV samples differ in sample collection interval and filter material (LV: poly-carbonate pore filter, 200 nm pore size; HV: quartz fibre filter). Concerning collection intervals, continuous sampling over eight hour intervals were chosen for the LV filters to resolve diurnal $N_{\mathrm{INP}}$ variations (non-detected). HV filters were collected during intervals of 24 h, interrupted by breaks due to the automatic shutdown

https://doi.org/10.5194/acp-2021-700
Preprint. Discussion started: 6 September 2021


Atmospheric Chemistry and Physics Discussions

to avoid contamination from ship exhaust. Possible low biases of $N_{\mathrm{INP}}$ for higher sampled volumes have been discussed in Bigg et al. (1963) and Mossop and Thorndike (1966), but do not reflect the trend found for our two sampling techniques. There could be an averaging effect from the longer sampling interval for the HV filters, when sampling from an unevenly distributed INP population. However, such effects require further investigation. The differences in filter material could be another factor, but are in contrast to Wex et al. (2020) finding good agreement between quartz fibre and poly-carbonate filters for identical sampling intervals. Contamination from ship exhaust should not effect INP analysis results (see Appendix C in Welti et al., 2020) as exhaust particles are not ice-active in the investigated temperature range. However, deactivation of some INP due to exhaust contamination can not be ruled out. For completeness, we report $N_{\mathrm{INP}}$ for HV sampling in Tab. S4. Due to a higher data coverage (LV: $n_{\mathrm{filter}} = 253$; HV: $n_{\mathrm{filter}} = 79$) allowing for more robust statistics, we decided to focus on LV samples for the in-depth analysis presented in the framework of the paper.

### 3.3 Analysis of sodium and MSA

Information on the aerosol chemical composition is widely used to infer the origin of the sampled population. The abundance of specific compounds is used as indication of source strength. The inevitable removal of aerosol particles from the atmosphere is taken into account by considering the atmospheric lifetime. To aid the characterisation of CCN and INP sources over the SO, sampled HV filters were analysed regarding the aerosol load and the atmospheric particle mass concentrations of sodium and MSA, two compounds known to be unaffected by stack exhaust.

On average, $32.4\,\mu g\,m^{-3}$ (median; IQR: 26.1–$49.6\,\mu g\,m^{-3}$) of $PM_{10}$ were observed during ACE (Tab. S5). Leg 1 exhibits a higher median value ($42.4\,\mu g\,m^{-3}$) compared to legs 2 and 3 (31.1 and $33.3\,\mu g\,m^{-3}$). Note that contrary to sodium and MSA (see subsection 2.3), an influence of the RV's ship exhaust on $PM_{10}$ mass can not be ruled out. However, the quantification of this potential influence is beyond the scope of this study.

Averaging sodium mass concentrations for the whole cruise gives a median value of $2.8\,\mu g\,m^{-3}$, with an IQR from 1.8–$3.9\,\mu g\,m^{-3}$ (Tab. S4). Higher median values for legs 1 and 3 compared to Leg 2 are found, similar to what is observed for $PM_{10}$. This is consistent with Blanchard and Woodcock (1957) showing SSA production to be driven by wave breaking and Schmale et al. (2019) showing on average higher wind speeds and significant wave heights for the legs with extended open ocean sections (legs 1 and 3). For the $34^{\mathrm{th}}$ Chinese National Antarctic and Arctic Research Expeditions (CHINARE) cruise on the SO (40–76° S, 170° E–110° W) in February–March 2018, Yan et al. (2020c) report an average sodium concentration of $0.8 \pm 0.8\,\mu g\,m^{-3}$ (mean $\pm$ SD). During Leg 2 of ACE, the part of the cruise that has the largest geographical overlap with the region covered during CHINARE, the median sodium mass concentration was $1.8\,\mu g\,m^{-3}$, i.e., more than two times higher than that observed during CHINARE.

MSA mass concentrations were generally 2 and 1 order of magnitude lower than the ones for $PM_{10}$ and sodium, respectively. Consequently, values are reported in $ng\,m^{-3}$ in the following. A median mass concentration of $102\,ng\,m^{-3}$ for the entire ACE cruise was found (Tab. S5), with highly variable values ranging from 1–$455\,ng\,m^{-3}$. Differences in median values between legs are very small. The highest concentration of $455\,ng\,m^{-3}$ was observed on the Ross Sea close to the Antarctic coast (Leg 2). Comparing our measurements of MSA with historical records, Davison et al. (1996) report for south of the Falkland islands

https://doi.org/10.5194/acp-2021-700
Preprint. Discussion started: 6 September 2021


Atmospheric Chemistry and Physics Discussions

in November 1992 a mean concentration of $27\,\mathrm{ng\,m^{-3}}$, with values ranging up to $99\,\mathrm{ng\,m^{-3}}$. During ACE in late February of 2017, values around $120\,\mathrm{ng\,m^{-3}}$ were found in this part of the SO between 70–36° W. Besides long-term trends over the last two decades, the difference of up to 1 order of magnitude might be due to the difference in season, with higher concentrations for ACE due to increased marine biological activity in early fall compared to late fall for Davison et al. (1996). Another factor is the large degree of variability in MSA abundance across the SO, depending on season and location as illustrated in Castebrunet et al. (2009), with values during ACE on the higher end of the scale. For a number of CHINARE Antarctic cruises, MSA concentrations are reported. Yan et al. (2020b) report for the polynya regions of the Ross Sea (50–78° S, 160–185° E) an average value of $44 \pm 22\,\mathrm{ng\,m^{-3}}$ (mean ± SD) for December of 2017 and $39 \pm 28\,\mathrm{ng\,m^{-3}}$ for January 2018. The maximum mass concentration of $211\,\mathrm{ng\,m^{-3}}$ was reported for the Ross Sea, at around 64–67° S, connected to the position of the dynamic sea ice edge at ∼64° S. Here, with the start of the sea ice melting in early December, the release of iron from ice into the water can spur marine microbial activity (Turner et al., 2004), that may result in an increased DMS emission and consequently secondary MSA production. Consistently, the maximum MSA mass concentration during ACE was encountered near the sea ice edge (∼70° S) of the Ross Sea in early February 2017. For the Amundsen Sea (40–76° S, 170° E–110° W) in February–March 2018 ($34^{\mathrm{th}}$ CHINARE cruise), average MSA concentrations of $31 \pm 17\,\mathrm{ng\,m^{-3}}$ are reported in Yan et al. (2020c). The ACE cruise went on the Amundsen Sea in early February 2017 and MSA concentrations in this region show a median value of $210\,\mathrm{ng\,m^{-3}}$. Overall, a difference in average MSA mass concentrations of up to 1 order of magnitude between our study and the CHINARE cruises becomes apparent. One factor might be the usage of different instrumentation and analysis techniques. Another factor, playing into the year-to-year variability, might be the presence of sea ice. Schmale et al. (2019) note a significantly lower sea ice extent on the Amundsen Sea during ACE, when compared to climatological records. The lack of a sea ice cover enables marine activity and the emission of aerosol precursors into the air. Adding to the encountered variability in MSA are besides aforementioned sources also the atmospheric sinks, e.g., precipitation that is associated with the frontal zones on the SO and efficiently removes MSA from the atmosphere, increasing the observed variability. For South Georgia, a sub-micron ($PM_1$) MSA mass of up to $200\,\mathrm{ng\,m^{-3}}$ was reported in Schmale et al. (2013). During ACE, the RV was on station close to this island in the beginning of March 2017, with MSA mass concentrations around $75\,\mathrm{ng\,m^{-3}}$ during these days, underlining the high variability in MSA abundance on the SO.

### 3.4 Correlation Analysis

The results of a correlation analysis performed with a selection of variables gathered during ACE is given as a Spearman rank correlation matrix in Fig. 9.

With regards to the results of our in situ aerosol particle measurement, $N_{\mathrm{total}}$ was found to be correlated with $N_{\mathrm{mode1}}$ (correlation coefficient $\rho = 0.9$, $p < .001$) and $N_{\mathrm{CCN,1.0}}$ ($\rho = 0.8$, $p < .001$). This mirrors the behaviour these quantities show in Fig. 2a, and is indicative for the importance of Aitken mode particles for the total particle and CCN number concentrations at high $SS$.

Correlations between sodium and mode 3 ($\rho = 0.7$, $p < .001$) as well as $PM_{10}$ ($\rho = 0.7$, $p < .001$) concentrations were found. As sodium is used as a conservative tracer for primary aerosol particles of marine origin (Legrand and Pasteur, 1998),

https://doi.org/10.5194/acp-2021-700
Preprint. Discussion started: 6 September 2021


Atmospheric Chemistry and Physics Discussions

especially sea salt, the correlations suggest that SSA significantly contributes to both, $PM_{10}$ and the coarse mode. However, we do not find a significant correlation between wind speed ($U_{10}$) and sodium mass concentration. Bates et al. (1998) attributed this kind of observation to the fact that the instantaneous wind speed at the RV is not representative for the conditions an air parcel experienced prior to its measurement. It is worth mentioning, that other studies on the SO found correlation between wind speed and sodium concentrations (e.g., Schmale et al., 2013; Yan et al., 2020a; Landwehr et al., 2021). Another factor might be, that the wind speed was averaged over $24\,\mathrm{h}$, in order to match the temporal resolution of the filter sampling. Possible short term effects might be lost due to the averaging process. Note, that the relative variability of the daily $U_{10}$ averages is between $0.7$ and $6\,\%$.

The particle concentration of mode 2 shows a positive correlation ($\rho \approx 0.7$) with $N_{\mathrm{CCN}}$ at $SS \leq 0.5\,\%$, pointing at the importance of accumulation mode particles for the CCN population at atmospheric relevant $SS$. No correlation was found between $N_{\mathrm{CCN}}$ and mode 3 number concentrations, suggesting little influence of SSA on the CCN population probed with our $SS$.

No correlation between $N_{\mathrm{CCN}}$ and MSA concentration was found. This seemingly contradicts findings of previous studies (e.g., Ayers and Gras, 1991) and our observations of the highest $N_{\mathrm{CCN}}$ (subsection 3.1) and the highest MSA concentration (subsection 3.3) occurring near the coast of Antarctica, and might be a smearing effect due to averaging. However, finding no correlation with our method does not imply that there could not be a connection under specific conditions and shorter time scales.

Furthermore, no correlation between $N_{\mathrm{CCN}}$ and in-water Chl-*a* or DMS concentration could be found, which is in line with Ayers et al. (1997). Considering the long process chain from in-water DMS to particles of CCN size this is not surprising and the argument that conditions at measurement point must not be representative for the conditions encountered by the air-parcel during transport in Bates et al. (1998) are very likely applicable.

Looking at $\kappa$ values, high correlation between different levels of supersaturation (except $SS = 1\,\%$) could be found, mirroring the lack of size-dependent composition presented in subsection 3.1. Further, no correlation between sodium concentration and $\kappa$ values was found, showing that the chemical information approximated by $\kappa$ is not connected to the mass-dominated results of the analysis of sodium and MSA. This again supports the observation of SSA particles not significantly contributing to the CCN population, as SSA dominates the sampled particle mass but not the particle number.

No correlations with any other variable was found for the MSA concentration. This includes the absence of the correlation between MSA and in-water DMS concentration. Although MSA is known to form exclusively from oxidation of DMS in the atmosphere (Sorooshian et al., 2007), a direct correlation is not expected. In-water DMS concentrations are not representative of DMS concentrations in the atmosphere (Ayers et al., 1997) and DMS has an atmospheric lifetime of several days over the SO (Chen et al., 2018).

INP concentrations measured at a temperature difference ($\Delta T$) of $4\,\mathrm{K}$ showed positive correlation ($\rho > 0.6$). This is expected, since these concentrations are cumulative along the temperature axis (see Fig. 8) and could indicate a common source that contributes INP over the $T$-range. For $\Delta T \geq 8\,\mathrm{K}$, only $N_{\mathrm{INP},-12}$ and $N_{\mathrm{INP},-20}$ show a correlation ($\rho = 0.7$, $p < .001$). This correlation between $N_{\mathrm{INP}}$ at $-12$ and $-20\,^{\circ}\mathrm{C}$ points at the importance of long-range transport and mixing influencing the

https://doi.org/10.5194/acp-2021-700
Preprint. Discussion started: 6 September 2021


Atmospheric Chemistry and Physics Discussions

INP population in the same way at both temperatures (Welti et al., 2018). The in-water Chl-*a* concentrations were also included in the correlation analysis, as it can be used as a proxy for biological activity (e.g., McCluskey et al., 2018). However, no direct correlation between $N_{\mathrm{INP}}$ and Chl-*a* was found. This suggests that the measured INP are not originating from local biogenic sources but does not exclude a delayed connection. In DeMott et al. (2010) a parameterization for $N_{\mathrm{INP}}$ is given that is based on $N_{500}$. We find no correlation between our measured $N_{\mathrm{INP}}$ and $N_{500}$, concluding that a parameterization based solely on $N_{500}$ is not applicable for the SO. No significant correlations were found between $N_{\mathrm{INP}}$ and $\mathrm{PM}_{10}$, $N_{\mathrm{total}}$ or any other physical and chemical properties measured. This clearly shows that trying to derive INP-related properties from bulk number-based or bulk mass-based aerosol properties without considering air mass history might lead to results not representative for atmospheric $N_{\mathrm{INP}}$. Instead, INP concentrations must be compared with results from methods selective to individual, rare particle types that could act as INP and the data must be segregated in terms of air mass properties or some other, more specific INP tracers such as mineral dust or proteins, to further elucidate INP sources.

## 4 Summary

During the Austral summer of 2016/17, we performed in situ measurements and filter sampling of $\mathrm{PM}_{10}$ aerosol particles for characterizing the physical and chemical properties of aerosol particles over the Southern Ocean during the Antarctic Circumnavigation Expedition. We focused on the abundance and properties of CCN and INP. A correlation analysis was performed to identify and interpret possible links between different aerosol physico-chemical parameters.

For the in situ measured aerosol particles, bi-modal aerosol particle number size distributions (PNSD) with a distinct Hoppel minimum between 50 and 80 nm were found (Fig. 2a). When the RV was close to continental land-masses, increased total particle ($N_{\mathrm{total}}$) and CCN number concentrations ($N_{\mathrm{CCN}}$) were observed (Fig. 2b). The absolute difference between $N_{\mathrm{total}}$ and $N_{\mathrm{CCN}}$ varied during the cruise and was associated with particle activation in the Aitken mode size range. This indicates an importance of the Aitken mode for the CCN population and cloud-formation. Generally, $N_{\mathrm{CCN}}$ spanned 2 orders of magnitude (e.g., at $SS = 0.3\,\%$ from roughly 3 to $590\,\mathrm{cm}^{-3}$), with the respective probability density functions (PDF) sharing resemblance with distributions in Schmale et al. (2018) for clean marine conditions of other locations around the globe. Averages of $N_{\mathrm{CCN}}$ per cruise leg (Fig. 3a) showed little difference between the legs and compare well ($<30\,\%$ percentage difference) with measurements of previous studies in the SO region. Values of the aerosol hygroscopicity parameter $\kappa$ were found to be in the range between 0.2 and 0.9, corresponding to mixtures with different amounts of organic and inorganic materials. Our $\kappa$ are about a factor of two lower than what was measured, e.g., over continental Antarctica or modelled for the SO region. Average values of $\kappa$ were found to be independent of $SS$ and thus particle size (Fig. 3b), indicating in first approximation an internally mixed CCN population in the Aitken and accumulation modes. The PDF of $\kappa$ values was found to be mono-modal for $SS = 0.15\,\%$ (Fig. 4c), while for higher $SS$ tails towards smaller $\kappa$ values were found, hinting at an increasing amount of organics in the smaller Aitken mode particles. In addition, tails towards higher $\kappa$ at $SS > 0.15\,\%$ indicate the occurrence of highly hygroscopic Aitken mode particles. The correlation analysis showed little-to-no connection between the CCN number concentration and quantities from the offline filter analysis, e.g., the concentrations of sodium and MSA (Fig. 9). This is due

https://doi.org/10.5194/acp-2021-700
Preprint. Discussion started: 6 September 2021


Atmospheric Chemistry and Physics Discussions

to the fact that the in situ measured aerosol properties considered here are governed by particle number, while the quantities determined from the filter samples (except for INP) are governed by particle mass. This often implies a focus on different size ranges. However, a connection was found through a positive correlation between total particle number concentration of the coarse mode and sodium mass concentration (Fig. 9). In addition, the absence of correlation between the sodium mass concentration and CCN number concentration clearly implies that SSA is not an important source of CCN. This agrees well with previous findings, e.g., in Schmale et al. (2019).

Analysis of filter-collected atmospheric aerosol samples for $N_{\mathrm{INP}}$ yielded temperature dependent concentrations between $-4$ and $-27^{\circ}\mathrm{C}$ (Fig. 8). Typically, the $N_{\mathrm{INP}}$ from one filter sample increased by 3 orders of magnitude within steps of $-10^{\circ}\mathrm{C}$. Time series of $N_{\mathrm{INP}}$ showed elevated values coinciding with the RV being in the proximity of land (Fig. 5). This points towards terrestrial and/or coastal sources influencing the INP population. Comparison with other studies (Fig. 5c) showed that our values are lower than what was observed previously over the SO (Bigg, 1973), while being on the upper end of what is reported in McCluskey et al. (2018) for a specific sector of the SO in March–April 2016 (Fig. 8). INP spectra (Fig. 8) for the most part of the cruise feature similar levels and temperature dependence of INP concentrations. The correlation analysis indicates correlations between $N_{\mathrm{INP}}$ in the temperature range between $-12$ and $-24^{\circ}\mathrm{C}$. We interpret this signal as indication that mixed long-range-transported populations of INP of biogenic origin ($T > -20^{\circ}\mathrm{C}$) and mineral dust ($T < -20^{\circ}\mathrm{C}$) were present. Indications for local INP sources are very rare, and no correlation between $N_{\mathrm{INP}}$ and Chl-*a*, as proxy for biological activity in the ocean, was found.

The results for the analysis of sodium and MSA in the sampled $\mathrm{PM}_{10}$ show that during ACE we encountered (mass-wise) a marine aerosol environment with typical SSA signals. Sodium concentrations showed a median of $2.8\,\mu\mathrm{g\,m^{-3}}$ (Tab. S5). A moderate positive correlation between sodium and $\mathrm{PM}_{10}$ (Fig. 9) underlined the importance of SSA for the sampled mass. During ACE, MSA concentrations were found to be highly variable, with a median of $102\,\mathrm{ng\,m^{-3}}$ (Tab. S5). Values were up to 1 order of magnitude higher than in comparable studies and seasonal variation seems to be one reason. The location of peak MSA concentrations near the sea ice edge is consistent with other studies. Similar patterns in the occurrence of maximum MSA concentrations and the hypothesised $\kappa$ value for MSA were found. However, a clear connection between MSA and CCN concentrations or $\kappa$ values did not show in our correlation analysis. With our data covering all sectors of the SO and the rich variety of atmospheric conditions encountered during the cruise, we conclude that such a connection might only be event-based.

The presented data set gives an unique, circum-Antarctic view on CCN and INP abundance, their properties and indications towards aerosol particle origin. Our data give insights into the conditions on the SO regarding cloud-relevant aerosol particles, compare well with previous studies and found already use in climate modelling (Regayre et al., 2020) and remote sensing applications (Efraim et al., 2020).

*Data availability.* The ACE data are available trough web portal ZENODO, with INP data from LV sampling under https://zenodo.org/record/2636777, CCN data under https://zenodo.org/record/2636765, and data on MSA and sodium under https://zenodo.org/record/3922147.

https://doi.org/10.5194/acp-2021-700
Preprint. Discussion started: 6 September 2021


Atmospheric Chemistry and Physics Discussions

INP data from HV sampling is available from the authors upon request. Further data sets are available at relevant citations within the manuscript.

*Author contributions.* CT performed the analysis and interpretation with contributions from SH, AW, JS, and FS. CT, SH, and FS wrote the manuscript. SH, AW, AB, JS, and MH performed the measurements during ACE. MGB and FS provided the in situ instrumentation. MvP provided the analysis of sodium and MSA of the filter samples. RM provided the PNSD data. All authors contributed to the writing and review of the manuscript.

*Competing interests.* The authors declare no competing interest.

*Acknowledgements.* ACE was a scientific expedition carried out under the auspices of the Swiss Polar Institute, supported by funding from the ACE Foundation and Ferring Pharmaceuticals. This work was supported by the Deutsche Forschungsgemeinschaft (DFG) in the framework of the priority programme “Antarctic Research with comparative investigations in the Arctic sea ice areas” SPP 1158 (grant STR 453/12-1). EU FP7 project "BACCHUS" (project number 603445) is acknowledged for financial support. Julia Schmale holds the Ingvar Kamrad Chair for Extreme Environments Research. Andrea Baccarini was supported by the Swiss National Science Foundation grant No. 169090. The authors would like to thank the PIs of ACE’s project 1, D. Antoine and S. Thomalla, for the chlorophyll a data. All data processing was performed using *Python* (version 2.7.14) on *Ipython* (version 5.4.1; Pérez and Granger, 2007). The correlation analysis was made possible by the *spearmanr* function of the *scipy.stats* package for *Python*. All figures in this study were created using the *Matplotlib* package for *Python* (Hunter, 2007).

https://doi.org/10.5194/acp-2021-700
Preprint. Discussion started: 6 September 2021


Atmospheric Chemistry and Physics Discussions

## References

Abram, N. J., Thomas, E. R., McConnell, J. R., Mulvaney, R., Bracegirdle, T. J., Sime, L. C., and Aristarain, A. J.: Ice core evidence for a 20th century decline of sea ice in the Bellingshausen Sea, Antarctica, Journal of Geophysical Research: Atmospheres, 115, https://doi.org/10.1029/2010JD014644, 2010.

Agresti, A. and Coull, B. A.: Approximate is better than "exact" for interval estimation of binomial proportions, The American Statistician, 52, 119–126, https://doi.org/10.1080/00031305.1998.10480550, 1998.

Albrecht, B. A.: Aerosols, cloud microphysics, and fractional cloudiness, Science, 245, 1227–1230, https://doi.org/10.1126/science.245.4923.1227, 1989.

Ayers, G. and Gras, J.: Seasonal relationship between cloud condensation nuclei and aerosol methanesulphonate in marine air, Nature, 353, 834–835, https://doi.org/10.1038/353834a0, 1991.

Ayers, G., Cainey, J., Gillett, R., and Ivey, J.: Atmospheric sulphur and cloud condensation nuclei in marine air in the Southern Hemisphere, Philosophical Transactions of the Royal Society of London. Series B: Biological Sciences, 352, 203–211, https://doi.org/10.1098/rstb.1997.0015, 1997.

Bates, T. S., Kapustin, V. N., Quinn, P. K., Covert, D. S., Coffman, D. J., Mari, C., Durkee, P. A., De Bruyn, W. J., and Saltzman, E. S.: Processes controlling the distribution of aerosol particles in the lower marine boundary layer during the First Aerosol Characterization Experiment (ACE 1), Journal of Geophysical Research: Atmospheres, 103, 16 369–16 383, https://doi.org/10.1029/97JD03720, 1998.

Bigg, E.: Ice nucleus concentrations in remote areas, Journal of the Atmospheric Sciences, 30, 1153–1157, https://doi.org/10.1175/1520-0469(1973)030<1153:INCIRA>2.0.CO;2, 1973.

Bigg, E., Mossop, S., Meade, R., and Thorndike, N.: The measurement of ice nucleus concentrations by means of Millipore filters, Journal of Applied Meteorology, 2, 266–269, https://doi.org/10.1175/1520-0450(1963)002<0266:TMOINC>2.0.CO;2, 1963.

Blanchard, D. and Woodcock, A.: Bubble formation and modification in the sea and its meteorological significance, Tellus, 9, 145–158, https://doi.org/10.3402/tellusa.v9i2.9094, 1957.

Carslaw, K., Lee, L., Reddington, C., Pringle, K., Rap, A., Forster, P., Mann, G., Spracklen, D., Woodhouse, M., Regayre, L., et al.: Large contribution of natural aerosols to uncertainty in indirect forcing, Nature, 503, 67, https://doi.org/10.1038/nature12674, 2013.

Castebrunet, H., Martinerie, P., Genthon, C., and Cosme, E.: A three-dimensional model study of methanesulphonic acid to non sea salt sulphate ratio at mid and high-southern latitudes, Atmospheric Chemistry and Physics, 9, 9449–9469, https://doi.org/10.5194/acp-9-9449-2009, 2009.

Chen, Q., Sherwen, T., Evans, M., and Alexander, B.: DMS oxidation and sulfur aerosol formation in the marine troposphere: a focus on reactive halogen and multiphase chemistry, Atmospheric Chemistry and Physics, 18, 13 617–13 637, https://doi.org/10.5194/acp-18-13617-2018, 2018.

Conen, F., Henne, S., Morris, C. E., and Alewell, C.: Atmospheric ice nucleators active $\geq -12^{\circ}$C can be quantified on $PM_{10}$ filters, Atmospheric Measurement Techniques, 5, 321–327, https://doi.org/10.5194/amt-5-321-2012, 2012.

Cornwell, G. C., Sultana, C. M., Prank, M., Cochran, R. E., Hill, T. C., Schill, G. P., DeMott, P. J., Mahowald, N., and Prather, K. A.: Ejection of dust from the ocean as a potential source of marine ice nucleating particles, Journal of Geophysical Research: Atmospheres, https://doi.org/10.1029/2020JD033073, 2020.

Covert, D. S., Kapustin, V. N., Quinn, P. K., and Bates, T. S.: New particle formation in the marine boundary layer, Journal of Geophysical Research: Atmospheres, 97, 20 581–20 589, https://doi.org/10.1029/92JD02074, 1992.

https://doi.org/10.5194/acp-2021-700
Preprint. Discussion started: 6 September 2021




Curran, M. A., van Ommen, T. D., Morgan, V. I., Phillips, K. L., and Palmer, A. S.: Ice core evidence for Antarctic sea ice decline since the 1950s, Science, 302, 1203–1206, https://doi.org/10.1126/science.1087888, 2003.

Dall'Osto, M., Ovadnevaite, J., Paglione, M., Beddows, D. C., Ceburnis, D., Cree, C., Cortés, P., Zamanillo, M., Nunes, S. O., Pérez, G. L., et al.: Antarctic sea ice region as a source of biogenic organic nitrogen in aerosols, Scientific reports, 7, 6047, https://doi.org/10.1038/s41598-017-06188-x, 2017.

Davison, B., O'Dowd, C., Hewitt, C., Smith, M., Harrison, R., Peel, D., Wolf, E., Mulvaney, R., Schwikowski, M., and Baltenspergert, U.: Dimethyl sulfide and its oxidation products in the atmosphere of the Atlantic and Southern Oceans, Atmospheric Environment, 30, 1895 – 1906, https://doi.org/10.1016/1352-2310(95)00428-9, joint 8th CAGCP and 2nd IGAC Conference on Global Atmospheric Chemistry, 1996.

de Leeuw, G., Andreas, E. L., Anguelova, M. D., Fairall, C. W., Lewis, E. R., O'Dowd, C., Schulz, M., and Schwartz, S. E.: Production flux of sea spray aerosol, Reviews of Geophysics, 49, https://doi.org/10.1029/2010RG000349, 2011.

DeMott, P. J., Prenni, A. J., Liu, X., Kreidenweis, S. M., Petters, M. D., Twohy, C. H., Richardson, M., Eidhammer, T., and Rogers, D.: Predicting global atmospheric ice nuclei distributions and their impacts on climate, Proceedings of the National Academy of Sciences, 107, 11 217–11 222, https://doi.org/10.1073/pnas.0910818107, 2010.

Dusek, U., Frank, G., Hildebrandt, L., Curtius, J., Schneider, J., Walter, S., Chand, D., Drewnick, F., Hings, S., Jung, D., et al.: Size matters more than chemistry for cloud-nucleating ability of aerosol particles, Science, 312, 1375–1378, https://doi.org/10.1126/science.1125261, 2006.

Efraim, A., Rosenfeld, D., Schmale, J., and Zhu, Y.: Satellite retrieval of cloud condensation nuclei concentrations in marine stratocumulus by using clouds as CCN chambers, Journal of Geophysical Research: Atmospheres, 125, https://doi.org/10.1029/2020JD032409, 2020.

Fossum, K. N., Ovadnevaite, J., Ceburnis, D., Dall'Osto, M., Marullo, S., Bellacicco, M., Simó, R., Liu, D., Flynn, M., Zuend, A., et al.: Summertime Primary and Secondary Contributions to Southern Ocean Cloud Condensation Nuclei, Scientific reports, 8, 13 844, https://doi.org/10.1038/s41598-018-32047-4, 2018.

Gong, X., Wex, H., van Pinxteren, M., Triesch, N., Fomba, K. W., Lubitz, J., Stolle, C., Robinson, T.-B., Müller, T., Herrmann, H., et al.: Characterization of aerosol particles at Cabo Verde close to sea level and at the cloud level–Part 2: Ice-nucleating particles in air, cloud and seawater, Atmos. Chem. Phys., 20, 1451–1468, https://doi.org/10.5194/acp-20-1451-2020, 2020.

Gras, J. L. and Keywood, M.: Cloud condensation nuclei over the Southern Ocean: wind dependence and seasonal cycles, Atmospheric Chemistry and Physics, 17, 4419–4432, https://doi.org/10.5194/acp-17-4419-2017, 2017.

Gysel, M. and Stratmann, F.: WP3-NA3: In-situ chemical, physical and optical properties of aerosols, Deliverable D3.11: Standardized protocol for CCN measurements, http://www.actris.net/Portals/97/Publications/quality%20standards/aerosol%20insitu/WP3_D3.13_M24_CCNC_SOP_v130514.pdf, 2014.

Hamilton, D. S., Lee, L. A., Pringle, K. J., Reddington, C. L., Spracklen, D. V., and Carslaw, K. S.: Occurrence of pristine aerosol environments on a polluted planet, Proceedings of the National Academy of Sciences, 111, 18 466–18 471, https://doi.org/10.1073/pnas.1415440111, 2014.

Hartmann, M., Blunier, T., Brügger, S. O., Schmale, J., Schwikowski, M., Vogel, A., Wex, H., and Stratmann, F.: Variation of ice nucleating particles in the European Arctic over the last centuries, Geophysical Research Letters, 46, 4007–4016, https://doi.org/10.1029/2019GL082311, 2019.

https://doi.org/10.5194/acp-2021-700
Preprint. Discussion started: 6 September 2021




Herenz, P., Wex, H., Mangold, A., Laffineur, Q., Gorodetskaya, I. V., Fleming, Z. L., Panagi, M., and Stratmann, F.: CCN measurements at the Princess Elisabeth Antarctica research station during three austral summers, Atmos. Chem. Phys., 19, 275–294, https://doi.org/10.5194/acp-19-275-2019, 2019.

Hoppel, W., Frick, G., and Larson, R.: Effect of nonprecipitating clouds on the aerosol size distribution in the marine boundary layer, Geophysical Research Letters, 13, 125–128, https://doi.org/10.1029/GL013i002p00125, 1986.

Humphries, R. S., Keywood, M. D., Gribben, S., McRobert, I. M., Ward, J. P., Selleck, P., Taylor, S., Harnwell, J., Flynn, C., Kulkarni, G. R., et al.: Southern Ocean latitudinal gradients of Cloud Condensation Nuclei, Atmospheric Chemistry and Physics Discussions, pp. 1–35, https://doi.org/10.5194/acp-2020-1246, 2021.

Hunter, J. D.: Matplotlib: A 2D graphics environment, Computing in Science & Engineering, 9, 90–95, https://doi.org/10.1109/MCSE.2007.55, 2007.

IPCC: Climate Change 2013: The Physical Science Basis. Contribution of Working Group I to the Fifth Assessment Report of the Intergovernmental Panel on Climate Change, Cambridge University Press, https://doi.org/10.1017/CBO9781107415324, 2013.

Khlystov, A., Stanier, C., and Pandis, S. N.: An Algorithm for Combining Electrical Mobility and Aerodynamic Size Distributions Data when Measuring Ambient Aerosol Special Issue of Aerosol Science and Technology on Findings from the Fine Particulate Matter Supersites Program, Aerosol Science and Technology, 38, 229–238, https://doi.org/10.1080/02786820390229543, 2004.

Köhler, H.: The nucleus in and the growth of hygroscopic droplets, Transactions of the Faraday Society, 32, 1152–1161, https://doi.org/10.1039/TF9363201152, 1936.

Kristensen, T., Müller, T., Kandler, K., Benker, N., Hartmann, M., Prospero, J., Wiedensohler, A., and Stratmann, F.: Properties of cloud condensation nuclei (CCN) in the trade wind marine boundary layer of the western North Atlantic, Atmospheric Chemistry and Physics, 16, 2675–2688, https://doi.org/10.5194/acp-16-2675-2016, 2016.

Landwehr, S., Thurnherr, I., Cassar, N., Gysel-Beer, M., and Schmale, J.: Using global reanalysis data to quantify and correct airflow distortion bias in shipborne wind speed measurements, Atmospheric Measurement Techniques, 13, 3487–3506, https://doi.org/10.5194/amt-13-3487-2020, 2020.

Landwehr, S., Volpi, M., Haumann, F. A., Robinson, C. M., Thurnherr, I., Ferracci, V., Baccarini, A., Thomas, J., Gorodetskaya, I., Tatzelt, C., Henning, S., Modini, R. L., Forrer, H. J., Lin, Y., Cassar, N., Simó, R., Hassler, C., Moallemi, A., Fawcett, S. E., Harris, N., Airs, R., Derkani, M. H., Alberello, A., Toffoli, A., Chen, G., Rodríguez Ros, P., Zamanillo, M., Cortés-Greus, P., Xue, L., Bolas, C. G., Leonard, K. C., Perez-Cruz, F., Walton, D., and Schmale, J.: Biogeochemistry and Physics of the Southern Ocean-Atmosphere System Explored With Data Science, Earth System Dynamics Discussions, 2021, 1–114, https://doi.org/10.5194/esd-2021-16, 2021.

Legrand, M. and Pasteur, E. C.: Methane sulfonic acid to non-sea-salt sulfate ratio in coastal Antarctic aerosol and surface snow, Journal of Geophysical Research: Atmospheres, 103, 10 991–11 006, https://doi.org/10.1029/98JD00929, 1998.

Lindzen, R. S.: Some coolness concerning global warming, Bulletin of the American Meteorological Society, 71, 288–299, http://www.jstor.org/stable/26227522, 1990.

McCluskey, C., Hill, T., Humphries, R., Rauker, A., Moreau, S., Strutton, P., Chambers, S., Williams, A., McRobert, I., Ward, J., et al.: Observations of ice nucleating particles over Southern Ocean waters, Geophysical Research Letters, 45, 11–989, https://doi.org/10.1029/2018GL079981, 2018.

McCoy, I. L., Bretherton, C. S., Wood, R., Twohy, C. H., Gettelman, A., Bardeen, C. G., and Toohey, D. W.: Influences of recent particle formation on Southern Ocean aerosol variability and low cloud properties, Journal of Geophysical Research: Atmospheres, 126, https://doi.org/10.1029/2020JD033529, 2021.



McFiggans, G., Artaxo, P., Baltensperger, U., Coe, H., Facchini, M. C., Feingold, G., Fuzzi, S., Gysel, M., Laaksonen, A., Lohmann, U., et al.: The effect of physical and chemical aerosol properties on warm cloud droplet activation, Atmospheric Chemistry and Physics, 6, 2593–2649, https://doi.org/10.5194/acp-6-2593-2006, 2006.

Moallemi, A., Landwehr, S., Robinson, C. M., Simó, R., Zamanillo, M., Chen, G., Baccarini, A., Schnaiter, M., Henning, S., Modini, R. L., et al.: Sources, Occurrence and Characteristics of Fluorescent Biological Aerosol Particles Measured over the Pristine Southern Ocean, Earth and Space Science Open Archive ESSOAr, https://doi.org/10.1002/essoar.10506321.1, 2021.

Modini, R. L., Frossard, A. A., Ahlm, L., Russell, L. M., Corrigan, C. E., Roberts, G. C., Hawkins, L. N., Schroder, J. C., Bertram, A. K., Zhao, R., Lee, A. K. Y., Abbatt, J. P. D., Lin, J., Nenes, A., Wang, Z., Wonaschütz, A., Sorooshian, A., Noone, K. J., Jonsson, H., Seinfeld, J. H., Toom-Sauntry, D., Macdonald, A. M., and Leaitch, W. R.: Primary marine aerosol-cloud interactions off the coast of California, Journal of Geophysical Research: Atmospheres, 120, 4282–4303, https://doi.org/10.1002/2014JD022963, 2015.

Mossop, S. and Thorndike, N.: The use of membrane filters in measurements of ice nucleus concentration. I. Effect of sampled air volume, Journal of Applied Meteorology, 5, 474–480, https://doi.org/10.1175/1520-0450(1966)005<0474:TUOMFI>2.0.CO;2, 1966.

Müller, K., Lehmann, S., Pinxteren, D. v., Gnauk, T., Niedermeier, N., Wiedensohler, A., and Herrmann, H.: Particle characterization at the Cape Verde atmospheric observatory during the 2007 RHaMBLe intensive, Atmospheric Chemistry and Physics, 10, 2709–2721, https://doi.org/10.5194/acp-10-2709-2010, 2010.

Murray, B. J., O'Sullivan, D., Atkinson, J. D., and Webb, M. E.: Ice nucleation by particles immersed in supercooled cloud droplets, Chem. Soc. Rev., 41, 6519–6554, https://doi.org/10.1039/C2CS35200A, 2012.

O'Dowd, C. D., Lowe, J. A., Smith, M. H., Davison, B., Hewitt, C. N., and Harrison, R. M.: Biogenic sulphur emissions and inferred non-sea-salt-sulphate cloud condensation nuclei in and around Antarctica, Journal of Geophysical Research: Atmospheres, 102, 12 839–12 854, https://doi.org/10.1029/96JD02749, 1997.

Pérez, F. and Granger, B. E.: IPython: a system for interactive scientific computing, Computing in Science & Engineering, 9, 21–29, https://doi.org/10.1109/MCSE.2007.53, 2007.

Petters, M. and Kreidenweis, S.: A single parameter representation of hygroscopic growth and cloud condensation nucleus activity, Atmos. Chem. Phys., 7, 1961–1971, https://doi.org/10.5194/acp-7-1961-2007, 2007.

Polen, M., Brubaker, T., Somers, J., and Sullivan, R. C.: Cleaning up our water: reducing interferences from nonhomogeneous freezing of "pure" water in droplet freezing assays of ice-nucleating particles, Atmospheric Measurement Techniques, 11, 5315–5334, https://doi.org/10.5194/amt-11-5315-2018, 2018.

Pringle, K., Tost, H., Pozzer, A., Pöschl, U., and Lelieveld, J.: Global distribution of the effective aerosol hygroscopicity parameter for CCN activation, Atmos. Chem. Phys., 10, 5241–5255, https://doi.org/10.5194/acp-10-5241-2010, 2010.

Quinn, P., Coffman, D., Johnson, J., Upchurch, L., and Bates, T.: Small fraction of marine cloud condensation nuclei made up of sea spray aerosol, Nature Geoscience, 10, 674, https://doi.org/10.1038/NGEO3003, 2017.

Quinn, P. K., Coffman, D. J., Kapustin, V. N., Bates, T. S., and Covert, D. S.: Aerosol optical properties in the marine boundary layer during the First Aerosol Characterization Experiment (ACE 1) and the underlying chemical and physical aerosol properties, Journal of Geophysical Research: Atmospheres, 103, 16 547–16 563, https://doi.org/10.1029/97JD02345, 1998.

Raes, F.: Entrainment of free tropospheric aerosols as a regulating mechanism for cloud condensation nuclei in the remote marine boundary layer, Journal of Geophysical Research: Atmospheres, 100, 2893–2903, https://doi.org/10.1029/94JD02832, 1995.

https://doi.org/10.5194/acp-2021-700
Preprint. Discussion started: 6 September 2021




Regayre, L. A., Schmale, J., Johnson, J. S., Tatzelt, C., Baccarini, A., Henning, S., Yoshioka, M., Stratmann, F., Gysel-Beer, M., Grosvenor, D. P., and Carslaw, K. S.: The value of remote marine aerosol measurements for constraining radiative forcing uncertainty, Atmos. Chem. Phys., 20, 10 063–10 072, https://doi.org/10.5194/acp-20-10063-2020, 2020.

Roberts, G. and Nenes, A.: A continuous-flow streamwise thermal-gradient CCN chamber for atmospheric measurements, Aerosol Science and Technology, 39, 206–221, https://doi.org/10.1080/027868290913988, 2005.

Rodriguez-Ros, P., Galí, M., Cortés, P., Robinson, C. M., Antoine, D., Wohl, C., Yang, M., and Simo, R.: Remote sensing retrieval of isoprene concentrations in the Southern Ocean, Earth and Space Science Open Archive, https://doi.org/10.1002/essoar.10502496.1, 2020.

Saliba, G., Sanchez, K. J., Russell, L. M., Twohy, C. H., Roberts, G. C., Lewis, S., Dedrick, J., McCluskey, C. S., Moore, K., DeMott, P. J., and Toohey, D. W.: Organic composition of three different size ranges of aerosol particles over the Southern Ocean, Aerosol Science and Technology, 0, 1–25, https://doi.org/10.1080/02786826.2020.1845296, 2020.

Sanchez, K. J., Roberts, G. C., Saliba, G., Russell, L. M., Twohy, C., Reeves, J. M., Humphries, R. S., Keywood, M. D., Ward, J. P., and McRobert, I. M.: Measurement report: Cloud processes and the transport of biological emissions affect southern ocean particle and cloud condensation nuclei concentrations, Atmos. Chem. Phys., 21, 3427–3446, https://doi.org/10.5194/acp-21-3427-2021, 2021.

Savoie, D. L. and Prospero, J. M.: Comparison of oceanic and continental sources of non-sea-salt sulphate over the Pacific Ocean, Nature, 339, 685–687, https://doi.org/10.1038/339685a0, 1989.

Schmale, J., Schneider, J., Nemitz, E., Tang, Y. S., Dragosits, U., Blackall, T. D., Trathan, P. N., Phillips, G. J., Sutton, M., and Braban, C. F.: Sub-Antarctic marine aerosol: dominant contributions from biogenic sources, Atmospheric Chemistry and Physics, 13, 8669–8694, https://doi.org/10.5194/acp-13-8669-2013, 2013.

Schmale, J., Henning, S., Henzing, B., Keskinen, H., Sellegri, K., Ovadnevaite, J., Bougiatioti, A., Kalivitis, N., Stavroulas, I., Jefferson, A., et al.: Collocated observations of cloud condensation nuclei, particle size distributions, and chemical composition, Scientific data, 4, 170 003, https://doi.org/10.1038/sdata.2017.3, 2017.

Schmale, J., Henning, S., Decesari, S., Henzing, B., Keskinen, H., Sellegri, K., Ovadnevaite, J., Pöhlker, M. L., Brito, J., Bougiatioti, A., et al.: Long-term cloud condensation nuclei number concentration, particle number size distribution and chemical composition measurements at regionally representative observatories, Atmospheric Chemistry and Physics, 18, 2853–2881, https://doi.org/10.5194/acp-18-2853-2018, 2018.

Schmale, J., Baccarini, A., Thurnherr, I., Henning, S., Efraim, A., Regayre, L., Bolas, C., Hartmann, M., Welti, A., Lehtipalo, K., Aemisegger, F., Tatzelt, C., Landwehr, S., Modini, R. L., Tummon, F., Johnson, J., Harris, N., Schnaiter, M., Toffoli, A., Derkani, M., Bukowiecki, N., Stratmann, F., Dommen, J., Baltensperger, U., Wernli, H., Rosenfeld, D., Gysel-Beer, M., and Carslaw, K.: Overview of the Antarctic Circumnavigation Expedition: Study of Preindustrial-like Aerosols and Their Climate Effects (ACE-SPACE), Bulletin of the American Meteorological Society, 0, null, https://doi.org/10.1175/BAMS-D-18-0187.1, 2019.

Sorooshian, A., Lu, M.-L., Brechtel, F. J., Jonsson, H., Feingold, G., Flagan, R. C., and Seinfeld, J. H.: On the source of organic acid aerosol layers above clouds, Environmental Science & Technology, 41, 4647–4654, https://doi.org/10.1021/es0630442, 2007.

Tobo, Y., Prenni, A. J., DeMott, P. J., Huffman, J. A., McCluskey, C. S., Tian, G., Pöhlker, C., Pöschl, U., and Kreidenweis, S. M.: Biological aerosol particles as a key determinant of ice nuclei populations in a forest ecosystem, Journal of Geophysical Research: Atmospheres, 118, 10 100–10 110, https://doi.org/10.1002/jgrd.50801, 2013.

Turner, S. M., Harvey, M. J., Law, C. S., Nightingale, P. D., and Liss, P. S.: Iron-induced changes in oceanic sulfur biogeochemistry, Geophysical Research Letters, 31, https://doi.org/10.1029/2004GL020296, 2004.

Twomey, S.: Pollution and the planetary albedo, Atmos. Environ., 8, 1251–1256, https://doi.org/10.1016/0004-6981(74)90004-3, 1974.

https://doi.org/10.5194/acp-2021-700
Preprint. Discussion started: 6 September 2021




Uetake, J., Hill, T. C., Moore, K. A., DeMott, P. J., Protat, A., and Kreidenweis, S. M.: Airborne bacteria confirm the pristine nature of the Southern Ocean boundary layer, Proceedings of the National Academy of Sciences, https://doi.org/10.1073/pnas.2000134117, 2020.

Vali, G.: Quantitative evaluation of experimental results an the heterogeneous freezing nucleation of supercooled liquids, Journal of the Atmospheric Sciences, 28, 402–409, https://doi.org/10.1175/1520-0469(1971)028<0402:QEOERA>2.0.CO;2, 1971.

van Pinxteren, M., Barthel, S., Fomba, K. W., Müller, K., Von Tümpling, W., and Herrmann, H.: The influence of environmental drivers on the enrichment of organic carbon in the sea surface microlayer and in submicron aerosol particles–measurements from the Atlantic Ocean, Elementa: Science of the Anthropocene, 5, 35, https://doi.org/10.1525/elementa.225, 2017.

Vergara-Temprado, J., Miltenberger, A. K., Furtado, K., Grosvenor, D. P., Shipway, B. J., Hill, A. A., Wilkinson, J. M., Field, P. R., Murray, B. J., and Carslaw, K. S.: Strong control of Southern Ocean cloud reflectivity by ice-nucleating particles, Proceedings of the National Academy of Sciences, 115, 2687–2692, https://doi.org/10.1073/pnas.1721627115, 2018.

Volpi, M., Landwehr, S., Thomas, J., and Schmale, J.: Distance to the nearest land/coastline (including small subantarctic islands) for the five-minute average cruise track of the Antarctic Circumnavigation Expedition (ACE) during the austral summer of 2016/2017., https://doi.org/10.5281/zenodo.3832045, 2020.

Walton, D. W. H. and Thomas, J.: Cruise Report - Antarctic Circumnavigation Expedition (ACE) 20th December 2016 - 19th March 2017, https://doi.org/10.5281/zenodo.1443511, 2018.

Wegener, A.: Thermodynamik der Atmosphäre, JA Barth, 1911.

Weingartner, E., Nyeki, S., and Baltensperger, U.: Seasonal and diurnal variation of aerosol size distributions (10< D< 750 nm) at a high-alpine site (Jungfraujoch 3580 m asl), Journal of Geophysical Research: Atmospheres, 104, 26 809–26 820, https://doi.org/10.1029/1999JD900170, 1999.

Welti, A., Müller, K., Fleming, Z. L., and Stratmann, F.: Concentration and variability of ice nuclei in the subtropical maritime boundary layer, Atmos. Chem. Phys., 18, 5307–5320, https://doi.org/10.5194/acp-18-5307-2018, 2018.

Welti, A., Bigg, E. K., DeMott, P. J., Gong, X., Hartmann, M., Harvey, M., Henning, S., Herenz, P., Hill, T. C. J., Hornblow, B., Leck, C., Löffler, M., McCluskey, C. S., Rauker, A. M., Schmale, J., Tatzelt, C., van Pinxteren, M., and Stratmann, F.: Ship-based measurements of ice nuclei concentrations over the Arctic, Atlantic, Pacific and Southern oceans, Atmos. Chem. Phys., 20, 15 191–15 206, https://doi.org/10.5194/acp-20-15191-2020, 2020.

Wex, H., Huang, L., Zhang, W., Hung, H., Traversi, R., Becagli, S., Sheesley, R. J., Moffett, C. E., Barrett, T. E., Bossi, R., et al.: Annual variability of ice-nucleating particle concentrations at different Arctic locations, Atmos. Chem. Phys., 19, 5293–5311, https://doi.org/10.5194/acp-19-5293-2019, 2019.

Wex, H., Jentsch, C., Mertes, S., Freney, E., and Stratmann, F.: Varitations in off-line filter sampling and analysis of Ice Nucleating Particle measurements, in: European Aerosol Conference, Aachen, Germany, 2020.

Wiedensohler, A., Birmili, W., Nowak, A., Sonntag, A., Weinhold, K., Merkel, M., Wehner, B., Tuch, T., Pfeifer, S., Fiebig, M., et al.: Mobility particle size spectrometers: harmonization of technical standards and data structure to facilitate high quality long-term observations of atmospheric particle number size distributions, Atmospheric Measurement Techniques, 5, 657–685, https://doi.org/10.5194/amt-5-657-2012, 2012.

Yan, J., Jung, J., Lin, Q., Zhang, M., Xu, S., and Zhao, S.: Effect of sea ice retreat on marine aerosol emissions in the Southern Ocean, Antarctica, Science of The Total Environment, 745, 140 773, https://doi.org/10.1016/j.scitotenv.2020.140773, 2020a.

https://doi.org/10.5194/acp-2021-700
Preprint. Discussion started: 6 September 2021


Atmospheric Chemistry and Physics Discussions

890 Yan, J., Jung, J., Zhang, M., Bianchi, F., Tham, Y. J., Xu, S., Lin, Q., Zhao, S., Li, L., and Chen, L.: Uptake selectivity of methanesulfonic acid (MSA) on fine particles over polynya regions of the Ross Sea, Antarctica, Atmospheric Chemistry and Physics, 20, 3259–3271, https://doi.org/10.5194/acp-20-3259-2020, 2020b.

Yan, J., Zhang, M., Jung, J., Lin, Q., Zhao, S., Xu, S., and Chen, L.: Influence on the conversion of DMS to MSA and $SO_4^{2-}$ in the Southern Ocean, Antarctica, Atmospheric Environment, 233, 117 611, https://doi.org/10.1016/j.atmosenv.2020.117611, 2020c.

https://doi.org/10.5194/acp-2021-700
Preprint. Discussion started: 6 September 2021


Atmospheric Chemistry and Physics Discussions

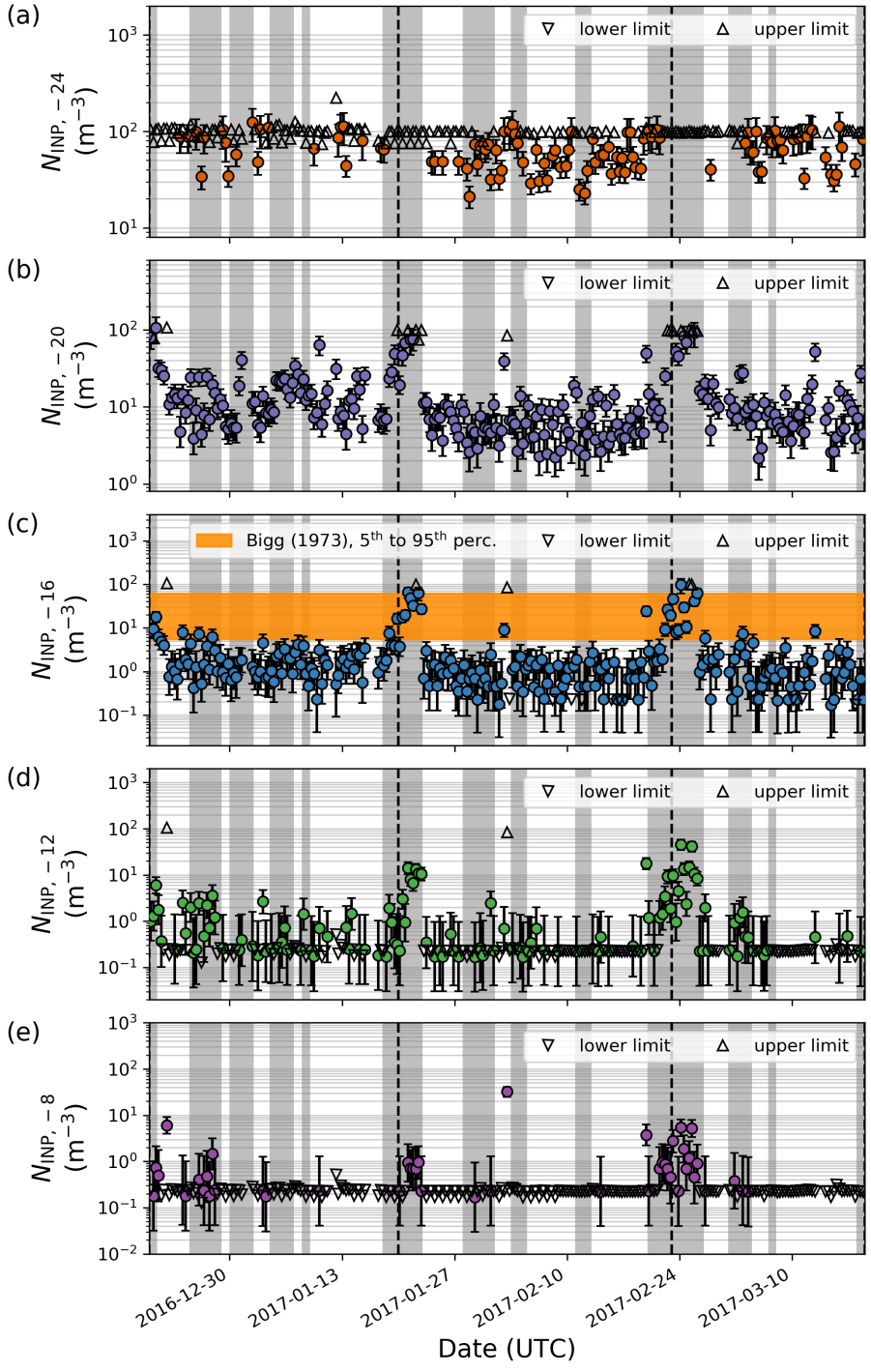


**Figure 5.** Time series of INP concentration ($N_{INP}$) at (a) −24, (b) −20, (c) −16, (d) −12, and (e) −8°C from filters sampled for eight hours each. Zero (infinite) values of $N_{INP}$ at given temperatures are presented as values of lower (upper) edge of the detectable range and indicated by downward (upward) triangles. The legs of ACE (dashed lines) and periods when the RV was close to land (grey area) are indicated. For reference, $N_{INP,-15}$ from Bigg (1973) are included in (c) as the range between their 5$^{th}$ and 95$^{th}$ percentile. A correction of the $N_{INP,-15}$ values from Bigg (1973) was applied, following the supporting information to McCluskey et al. (2018).

https://doi.org/10.5194/acp-2021-700
Preprint. Discussion started: 6 September 2021


Atmospheric Chemistry and Physics Discussions

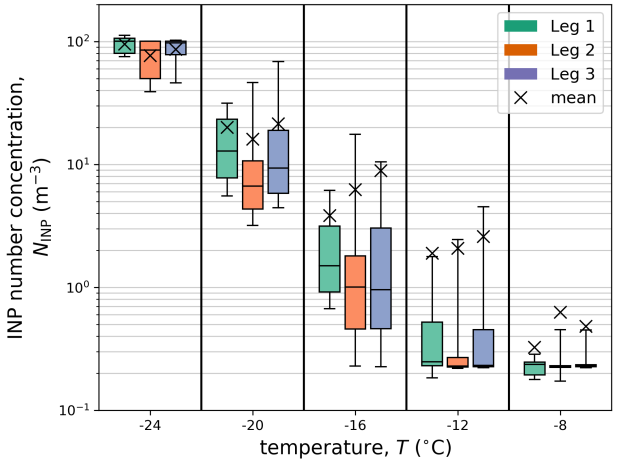


**Figure 6.** Mean values (crosses) and box-and-whiskers plots indicating the median (horizontal lines), inter-quartile range (boxes), and $10^{\text{th}}$ to $90^{\text{th}}$ percentiles (whiskers) of INP concentration ($N_{\text{INP}}$) derived from filters sampled for 8 h during ACE's Leg 1 (green), Leg 2 (orange), and Leg 3 (purple). Averaging was performed by treating zero (infinite) values of $N_{\text{INP}}$ at given temperature as values of the lower (upper) limit of the detectable range.

https://doi.org/10.5194/acp-2021-700
Preprint. Discussion started: 6 September 2021


Atmospheric Chemistry and Physics Discussions

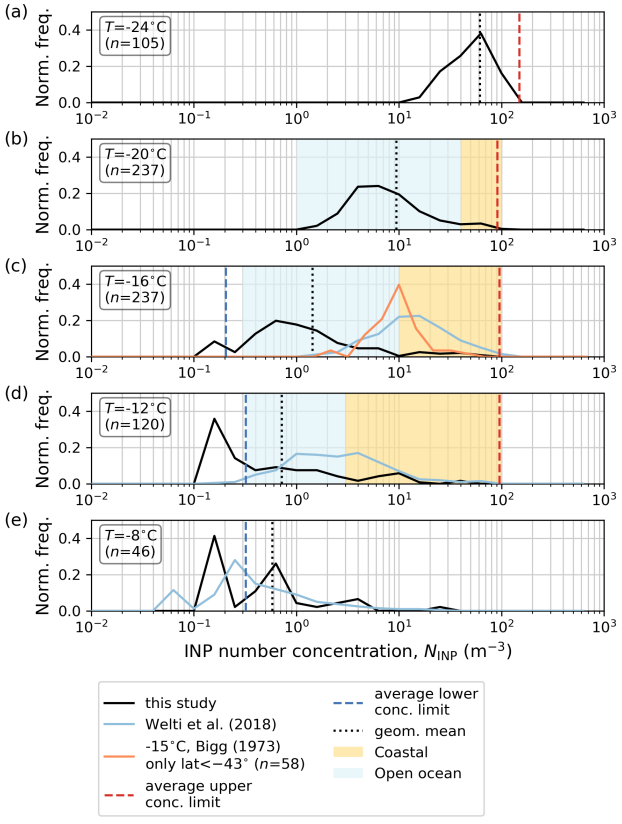


**Figure 7.** Normalized probability density functions (solid) and geometric mean values (dotted) for INP concentrations ($N_{\mathrm{INP}}$) at (a) $-24$, (b) $-20$, (c) $-16$, (d) $-12$ and (e) $-8\,^{\circ}\mathrm{C}$ are given for filters sampled for 8 h (black). For reference, $N_{\mathrm{INP},-16}$ , $N_{\mathrm{INP},-12}$, and $N_{\mathrm{INP},-8}$ for Cabo Verde (North Atlantic; Welti et al., 2018) are given in (c), (d), and (e), respectively (blue). Additionally, $N_{\mathrm{INP},-15}$ from Bigg (1973) for data points south of $43^{\circ}$ S (orange) is given for comparison. A classification of modes by sampling location is given (yellow: coastal; light blue: open ocean) and averages of the upper (dark red) and lower concentration limit (dark blue) is indicated by dashed lines. The number of data points ($n$) is indicated in the Fig.

https://doi.org/10.5194/acp-2021-700
Preprint. Discussion started: 6 September 2021


Atmospheric Chemistry and Physics Discussions

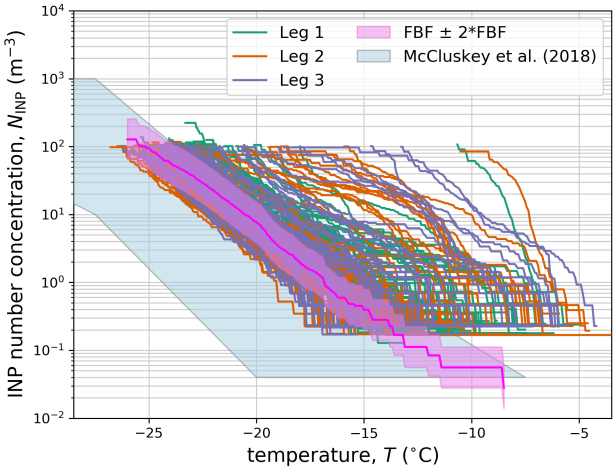


**Figure 8.** INP concentrations ($N_{\mathrm{INP}}$) as function of temperature ($T$) from LV filters sampled during ACE. The measurement background from averaged spectra of field blank filters (FBF) ± a factor of two is indicated (pink line and area). For comparison, the data range from McCluskey et al. (2018) (light blue) is given.

https://doi.org/10.5194/acp-2021-700
Preprint. Discussion started: 6 September 2021


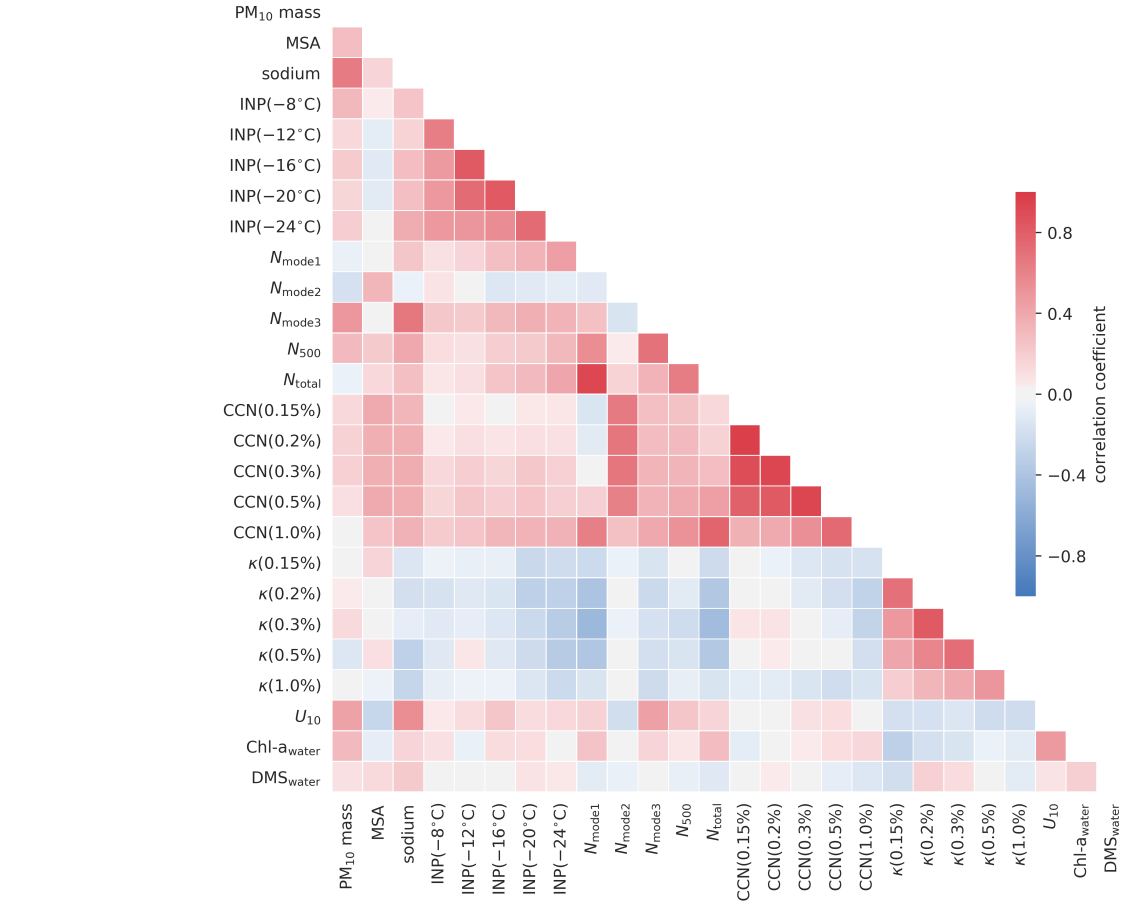


**Figure 9.** Spearman rank correlation matrix of quantities directly measured or derived from measurements during ACE. From the 24 h long HV sampling, $PM_{10}$ mass and mass concentrations of particulate sodium and MSA are included. INP number concentrations at temperatures of $-8$, $-12$, $-16$, $-20$, and $-24^{\circ}$C (INP($T$)) are included from the LV filters, sampling for eight hours. Here, the estimates for INP concentrations above and below the detection limit are included. From hourly smoothed particle number size distributions, the total particle number concentration ($N_{\mathrm{total}}$), respective three modes ($N_{\mathrm{mode1}}$, $N_{\mathrm{mode2}}$, and $N_{\mathrm{mode3}}$), and the number concentration of particles larger 500 nm in diameter ($N_{500}$) are included. CCN number concentration at 0.15, 0.2, 0.3, 0.5, and 1 % supersaturation (CCN($SS$)) and derived aerosol particle hygroscopicity parameter ($\kappa(SS)$) are included. Additionally, daily-averaged wind speed at 10ma.s.l. ($U_{10}$), and in-water concentrations of chlorophyll-a (Chl-$a_{\mathrm{water}}$) and dimethyl sulfide ($\mathrm{DMS}_{\mathrm{water}}$) are used. Positive correlation between two quantities indicates a similar trend over time, while an opposing behaviour is indicated by a negative correlation coefficient.